CELL AND TISSUE-SPECIFIC GENES WITH T-DMRS

In mammalian embryogenesis, the first differentiation event that determines lineage of the trophectoderm and inner cell mass (ICM) occurs during the blastocyst stage. Embryonic stem (ES) cells established from ICM are pluripotent and can contribute to all ICM lineages.[41,42] Trophoblast stem (TS) cells, established from trophectoderm, have the ability to differentiate into trophoblast lineage in vitro.[43]

The *Oct-4* gene, a POU family transcription factor, is expressed in the oocyte and preimplantation embryo, but expression is restricted later to ICM of the blastocyst.[44–46] The *Oct-4* gene has a CG-rich and TATA-less promoter.[46,47] In *Oct-4*-deficient embryos, ICM loses pluripotency and trophoblast cells do not proliferate to develop the placenta.[48] The *Oct-4* gene is expressed in ES cells but not in TS cells.[43] Reduction of *Oct-4* gene expression induces transdifferentiation of ES cells into TS cells under certain culture conditions.[49] Based on these observations, the *Oct-4* gene seems the master gene that determines pluripotency and differentiation of these stem cells. There is a T-DMR in the upstream regulatory region of the *Oct-4* gene that is hypomethylated in ES cells but hypermethylated in TS cells.[50] In addition, the *Oct-4* region is associated with hyperacetylated histones in ES cells in contrast to TS cells,[50] implying that DNA methylation status is correlated with chromatin structure of the *Oct-4* gene.

Nanog gene encodes for another transcription factor involved in the multipotency of ES cells.[51]*Nanog* gene has a T-DMR and is regulated by DNA methylation and histone modifications.[52] Expression of master transcription factors such as *Oct-4* and *Nanog*, which govern early development and differentiation, has been used as a marker for stem cells including ES cells and induced pluripotent stem (iPS) cells.[53,54]

In addition to *Oct-4* and *Nanog*, some tissue-specific genes with poor CpGs in promoter regions have T-DMRs. Expression of *rPL-1* is tissue specific and strictly limited to trophoblast giant cells of the placenta.[55] In the *rPL-1* gene promoter, a T-DMR exists that consists of only 17 CpG sites in the 3.4-kb section of the 5'-flanking region. The T-DMR of *rPL-1* is hypomethylated specifically in the placenta, and hypermethylated in other tissues.[56] Thus tissue-specific restricted expression of *rPL-1* is controlled by methylation of CpGs.

The *Sry* gene, which encodes a master protein that initiates testis differentiation in mammals,[57] also has a T-DMR.[58] In mice, expression of *Sry* is restricted to gonadal somatic cells at 10.5–12.5 days postcoitum (dpc). The T-DMR is hypermethylated in 8.5-dpc embryos, when *Sry* gene expression is not observed, and hypomethylated only at 11.5 dpc. Although there are only 8 CpGs in the 2-kb upstream region of the linear form of *Sry*, methylation of this small number of CpGs regulates spatiotemporal expression of the *Sry* gene.

Thus, various types of tissue-specific genes are under epigenetic regulation regardless of CpG content. These genes encode transcription factors, enzymes, and hormones as described above.

TISSUE/CELL TYPE-SPECIFIC DNA METHYLATION PROFILES

The human genome project uncovered 30,000 genes and approximately 29,000 CpG islands,[22,23] and there are 30,000 genes and 15,000 CpG islands in the mouse genome.[24] It is reported that 50% of CpG islands are linked to tissue-specific genes.[59] How many loci are differentially methylated or unmethylated during development and within different tissues?

Restriction landmark genomic scanning, used for genome-wide DNA methylation analysis, enables us to focus on thousands of T-DMRs and analyze comprehensively methylation status of the entire genome.[60–62] We previously analyzed genomes from 10 different cell types and tissues including ES cells and TS cells. When 1500 loci of 10 cell/tissue types were analyzed, there were 247 T-DMRs, and importantly, the unique methylation status of each tissue and cell type was observed at these 247 T-DMRs.[15] The DNA methylation profiles clearly show that differentiation involves massive alteration of methylation status, with both methylation and demethylation changes occurring at genome-wide multiple loci.

Taken together, these findings indicate that each cell/tissue type has a specific DNA methylation profile at T-DMRs (Fig. 2). The DNA methylation profile is specific to cell and tissue type, much like a fingerprint is distinct, and can be used as an identification tag for cells. The DNA methylation profile also provides a novel method to evaluate similarities of cells because it reflects the similarity in patterns of various lineages during differentiation.[63] Because DNA methylation profile is a unique identification tag for cells, a change in the DNA methylation profile will cause an alteration in cell properties.

EPIGENOME: GENOME-WIDE EPIGENETICS

Genome-wide epigenetic information is called the epigenome. Recently, we developed D-REAM, a genome-wide DNA methylation analysis method for T-DMR profiling using restriction tag–mediated amplification combined with microarray technology.[40] Previously, genome-wide DNA methylation analyses such as restriction landmark genomic scanning were performed using restriction enzyme *NotI* or *HapII*, whose targets are located mainly at CpG islands. In contrast, D-REAM uses *HpyCH4IV*, a methylation-sensitive restriction enzyme whose recognition sites are distributed throughout the mouse genome in a less biased manner than that of *HapII* and *NotI*. Therefore, D-REAM was developed as a low-bias method. Another advantage is that D-REAM is more flexible than other methods because it enables selective amplification of DNA fragments digested with any restriction enzyme. Our experience indicates that D-REAM is more effective at providing detailed methylation profiles than previously available methods.[40]

We performed D-REAM using a mouse promoter tiling array covering a region from −6 to 2.5 kb (−30,000 transcription start sites) and revealed 3000 T-DMRs that were hypomethylated in liver compared with in cerebrum. The DNA methylation profile of liver was distinct from that of kidney and spleen.[40] Furthermore, tissue-specific expression of genes with T-DMRs was highly correlated with liver

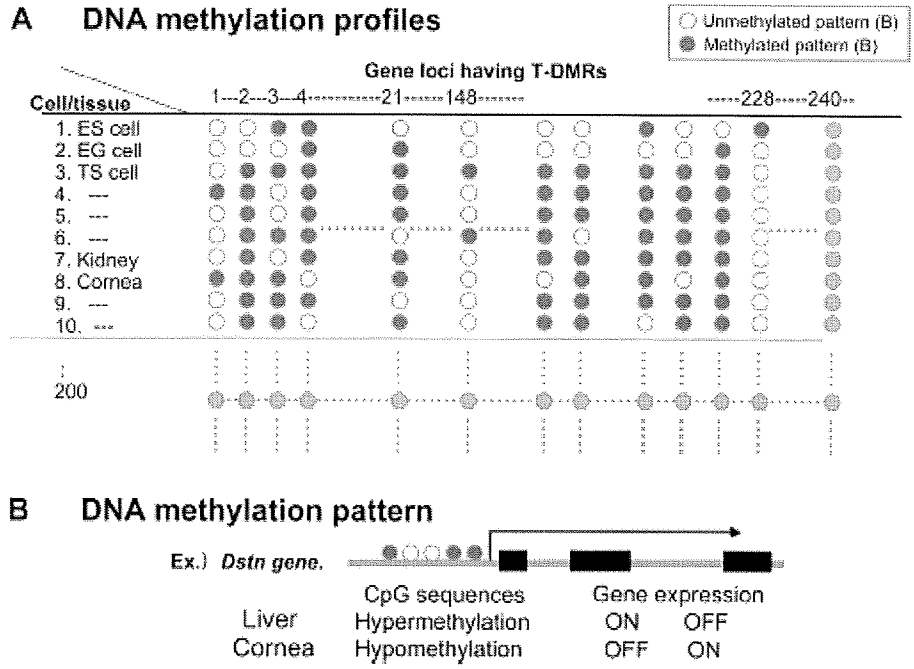

FIGURE 2. Cell type–specific and tissue type–specific DNA methylation profiles comprising DNA methylation patterns of T-DMARs. For example, focusing on mouse *Dstn* gene, a DNA methylation pattern in cornea is different from that of liver. A, These patterns constitute cell/tissue-specific DNA methylation profiles. The DNA methylation profile of a cell type is unique and can be a novel tool to define and characterize the cell type. B, Each cell/tissue has a unique pattern of DNA methylation status at each T-DMR.

hypomethylation status, indicating that DNA methylation profile reflects tissue-specific gene expression profile. D-REAM analysis revealed that T-DMRs are located a few kilobases both upstream and downstream of the transcription start sites. Previous studies to locate T-DMRs have focused on the promoter region only. Although preferential tissue-specific expression of non–CpG island genes has been reported previously, D-REAM confirmed that hypomethylation and gene expression are observable in CpG island genes as well, as discussed above.[40]

D-REAM analysis was used to identify T-DMRs, which could provide investigative insight into the roles of genome-wide DNA methylation. T-DMR profiles are tissue specific and facilitate tissue identification by reflecting tissue-specific gene function. The multilayered regulation of tissue-specific gene function could be elucidated by DNA methylation tissue profiling.[40]

EPIGENETIC BASIS OF HUMAN DISEASES

Aging is characterized as a time-dependent decline in responsiveness or adaptation to the environment. The loss of phenotypic plasticity could be mediated epigenetically. Loss of the normal balance between gene promoting/silencing factors could occur throughout the genome during the process of aging. Indeed, evidence is accumulating that the epigenome is an important target of internal and external environmental factors such as toxins, growth factors, dietary methyl donors, and so on.[64,65] The human genome encodes approximately 30,000 genes, as mentioned previously,[22,23] that are expressed in specific cells at precise times according to cell type–specific DNA methylation profiles. In addition to primary genetic mutations, epimutations, detectable as aberrant epigenetic status, should be considered as a process of gene deregulation. Disruptions of DNA methylation profiles, that putatively produce abnormal cells and tissues, might help to explain how particular diseases—especially age-dependent diseases—can occur and why common diseases increase generally in an age-dependent manner. Thus, changes in DNA methylation profiles could impact on human health, and epigenetic mechanisms might gain new perspective in human diseases related to gene deregulation, as shown in Fig. 3.

Recent developments in corneal genetics (Table 1)[66–81] have led to implementation of a new classification scheme that takes into account the responsible gene defect, particularly the tissue growth factor beta inducible (TGFBI) group in the case of corneal dystrophy, rather than simply by clinical appearance.[6,82] It is feasible that a single gene such as *TGFBI* can be silenced by DNA methylation and DNA mutation, resulting in disease.

We are now confronted with even more questions about the role of genetic background and environmental influences in the phenotypic expression of corneal dystrophies. Clinicians will be able to use molecular genetic analysis to confirm or refute presumptive clinical diagnoses in cases of suspected dystrophic corneal disorders. Indeed, we have already found T-DMRs (Fig. 2) in several genes as listed in Table 1.[66–81] Therefore, in future, it is possible that DNA methylation profiles in corneal tissues could become effective clinical diagnostic tools in corneal dystrophies if epigenetic modification occurs on the genes associated with corneal disorders.

CONCLUSIONS

Numerous genes, which are tissue/cell type specifically expressed, are regulated by epigenetics. Methylation of DNA,

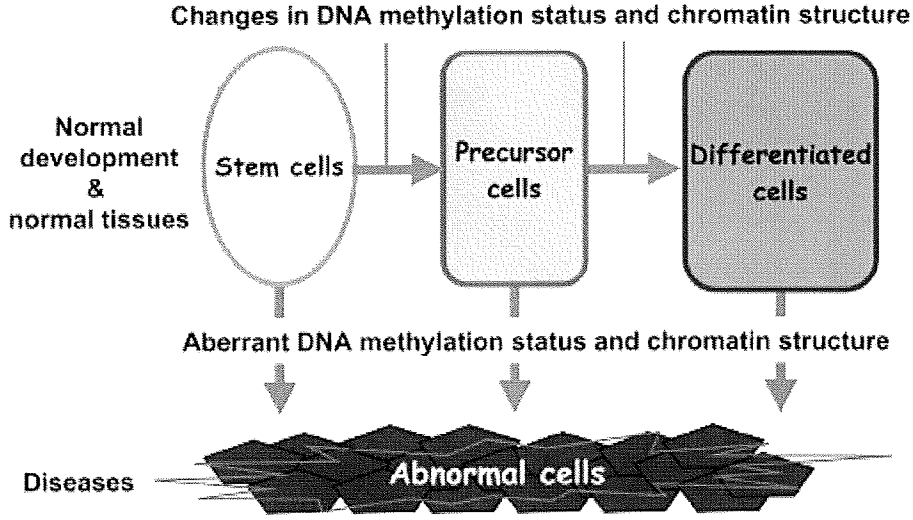

FIGURE 3. Aberrant DNA methylation status and chromatin remodeling cause diseases through producing abnormal cells. The genome encodes must be expressed according to cell type–specific DNA methylation profiles. In addition to primary genetic mutations, epimutations putatively produce abnormal cells and tissues, which might cause diseases.

associated with chromatin configuration changes, is the intermediate regulatory phase of gene expression and occurs between a stable genome and a rapidly changeable transcriptome (Fig. 4). Epigenetics is the study of this "cellular memory of gene expression" that results in maintenance of various cell types. Genome-wide DNA methylation profiles, which consist of information on methylation patterns of numerous loci, store the "cellular memory" that governs tissue/cell type features. Various environmental factors affect DNA methylation profiles, and their abnormalities seem involved in various diseases. Epigenetics is an emerging paradigm that explains various normal and abnormal biological phenomena from novel viewpoints. Tissue/cell type–specific DNA methylation profiles, vehicles of epigenetic memory, could be useful tools in understanding health and disease. Epigenetics and epigenome analysis will provide distinct approaches for facilitating novel advances in diagnosis and treatment and drug development for various diseases, including corneal disorders.

ACKNOWLEDGMENTS

We gratefully thank Dr. Akihiro Ikeda and Dr. Sakae Ikeda (University of Wisconsin-Madison) for discussion and Dr. Maddy Roberts for proofreading the article.

TABLE 1. Summary of Corneal Disorders With Gene

Gene	Locus	Inheritance	Dystrophy	Layer	Reference
TGFBI	5q31	AD	RBD	Bowman	Kannabiran and Klintworth[66]
			Thiel-Behnkel	Bowman	
			GCD	Stromal	
			Lattice (LCD) type I	Stromal	
Dstn	2(mouse)	AR	Corneal surface disease	Epithelial	Ikeda et al[67]; Verdoni et al[68]
KRT3	12q13	AD	Meesman	Epithelial	Irvine et al[69]; Nishida et al[70]
KRT12	17q12	AD	Meesman	Epithelial	Irvine et al[69]; Nishida et al[70]
Gelsolin	9q34	AD	Lattice (LCD) type II	Stromal	Rodrigues et al[71]
Decorin	12q22	AD	CHSD	Stromal	Bredrup et al[72]
PIP5K3	2q35	AD	Fleck (CFD)	Stromal	Li et al[73]
MIS1	1q32	AR	GDLD	Stromal	Tsujikawa et al[74]; Tasa et al[75]
CHST6	16q22	AR	MCD	Stromal	Akama et al[76]
CYP4V2	4q35	AR	BCD	Stromal	Li et al[77]
COL8A2	1p23.3–1p32	AD	FECD	Endothelial	Biswas et al[78]; Gottsch et al[79]
SLC4A11	20p11.2-20q11.2	AR	CHED type II	Endothelial	Vithana et al[80]
TCF8	10p11-10q11	AD	PPCD	Endothelial	Krafchak et al[81]

AD, autosomal dominant; AR, autosomal recessive; BCD, Bietti corneal dystrophy; CFD, corneal fleck dystrophy; CHED, congenital hereditary endothelial dystrophy; CHSD, congenital hereditary stromal dystrophy; FECD, Fuchs endothelial corneal dystrophy; GCD, granular corneal dystrophy; GDLD, gelatinous drop-like dystrophy; LCD, lattice corneal dystrophy; MCD, macular corneal dystrophy; PPCD, posterior polymorphous corneal dystrophy; RBD, Reis–Bucklers dystrophy.

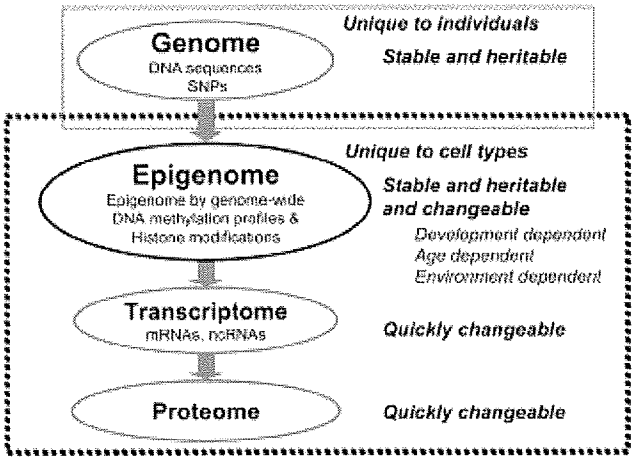

FIGURE 4. Genetic information flow with epigenetics.

REFERENCES

1. Russo U, Martienssen R, Riggs AD. *Epigenetic Mechanisms of Gene Regulation*. Woodbury, NY: Cold Spring Harbor Laboratory Press; 1996: 1–4.
2. Lieb JD, Beck S, Bulyk ML, et al. Applying whole-genome studies of epigenetic regulation to study human disease. *Cytogenet Genome Res*. 2006;114:1–15.
3. Kaplan J. Genomics and medicine: hopes and challenges. *Gene Ther*. 2002;9:658–661.
4. Murphy R, Ellard S, Hattersley AT. Clinical implications of a molecular genetic classification of monogenic beta-cell diabetes. *Nat Clin Pract Endocrinol Metab*. 2008;4:200–213.
5. Puddu P, Puddu GM, Cravero E, et al. The genetic basis of essential hypertension. *Acta Cardiol*. 2007;62:281–293.
6. Poulaki V, Colby K. Genetics of anterior and stromal corneal dystrophies. *Semin Ophthalmol*. 2008;23:9–17.
7. Voisey J, Morris CP. SNP technologies for drug discovery: a current review. *Curr Drug Discov Technol*. 2008;5:230–235.
8. Bird AP. Use of restriction enzymes to study eukaryotic DNA methylation. II. The symmetry of methylated sites supports semi-conservative copying of the methylation pattern. *J Mol Biol*. 1978;118: 49–60.
9. Gruenbaum Y, Stein R, Cedar H, et al. Methylation of CpG sequences in eukaryotic DNA. *FEBS Lett*. 1981;124:67–71.
10. Cubas P, Vincent C, Coen E. An epigenetic mutation responsible for natural variation in floral symmetry. *Nature*. 1999;401:157–161.
11. Kouzarides T. Chromatin modifications and their function. *Cell*. 2007; 128:693–705.
12. Bird A. DNA methylation patterns and epigenetic memory. *Genes Dev*. 2002;16:6–21.
13. Shiota K. DNA methylation profiles of CpG islands for cellular differentiation and development in mammals. *Cytogenet. Genome Res*. 2004;105:325–334.
14. Ikegami K, Ohgane J, Tanaka S, et al. Interplay between DNA methylation, histone modification and chromatin remodeling in stem cells and during development. *Int J Dev Biol*. 2009;53:203–214.
15. Shiota K, Kogo Y, Ohgane J, et al. Epigenetic marks by DNA methylation specific to stem, germ and somatic cells in mice. *Genes Cells*. 2002;7: 961–969.
16. Li E, Bestor TH, Jaenisch R. Targeted mutation of the DNA methyltransferase gene results in embryonic lethality. *Cell*. 1992;69: 915–926.
17. Okano M, Bell DW, Haber DA, et al. DNA methyltransferases Dnmt3a and Dnmt3b are essential for de novo methylation and mammalian development. *Cell*. 1999;99:247–257.
18. Okamoto I, Arnaud D, Le Baccon P, et al. Evidence for de novo imprinted X-chromosome inactivation independent of meiotic inactivation in mice. *Nature*. 2005;438:369–373.
19. Bourc'his D, Xu GL, Lin CS, et al. Dnmt3L and the establishment of maternal genomic imprints. *Science*. 2001;294:2536–2539.
20. Kaneda M, Okano M, Hata K, et al. Essential role for de novo DNA methyltransferase Dnmt3a in paternal and maternal imprinting. *Nature*. 2004;429:900–903.
21. Morgan HD, Santos F, Green K, et al. Epigenetic reprogramming in mammals. *Hum Mol Genet*. 2005;14:R47–R58.
22. Lander ES, Linton LM, Birren B, et al. Initial sequencing and analysis of the human genome. *Nature*. 2001;409:860–921.
23. Venter JC, Adams MD, Myers EW, et al. The sequence of the human genome. *Science*. 2001;291:1304–1351.
24. Waterston RH, Lindblad-Toh K, Birney E, et al. Initial sequencing and comparative analysis of the mouse genome. *Nature*. 2002;420:520–562.
25. Razin A, Szyf M. DNA methylation patterns. Formation and function. *Biochim Biophys Acta*. 1984;782:331–342.
26. Cross SH, Bird AP. CpG islands and genes. *Curr Opin Genet Dev*. 1995;5: 309–314.
27. Ko YG, Nishino K, Hattori N, et al. Stage-by-stage change in DNA methylation status of Dnmt1 locus during mouse early development. *J Biol Chem*. 2005;280:9627–9634.
28. Bird AP. CpG-rich islands and the function of DNA methylation. *Nature*. 1986;321:209–213.
29. Gardiner-Garden M, Frommer M. CpG islands in vertebrate genomes. *J Mol Biol*. 1987;196:261–282.
30. Takai D, Jones PA. Comprehensive analysis of CpG islands in human chromosomes 21 and 22. *Proc Natl Acad Sci U S A*. 2002;99:3740–3745.
31. Larsen F, Gundersen G, Lopez R, et al. CpG islands as gene markers in the human genome. *Genomics*. 1992;13:1095–1107.
32. Yen PH, Patel P, Chinault AC, et al. Differential methylation of hypoxanthine phosphoribosyltransferase genes on active and inactive human X chromosomes. *Proc Natl Acad Sci U S A*. 1984;81:1759–1763.
33. Bird A, Taggart M, Frommer M, et al. A fraction of the mouse genome that is derived from islands of nonmethylated, CpG-rich DNA. *Cell*. 1985; 40:91–99.
34. De Smet C, Lurquin C, Lethe B, et al. DNA methylation is the primary silencing mechanism for a set of germ line- and tumor-specific genes with a CpG-rich promoter. *Mol Cell Biol*. 1999;19:7327–7335.
35. Imamura T, Ohgane J, Ito S, et al. CpG island of rat sphingosine kinase-1 gene: tissue-dependent DNA methylation status and multiple alternative first exons. *Genomics*. 2001;76:117–125.
36. Spiegel S, Milstien S. Sphingosine-1-phosphate: an enigmatic signalling lipid. *Nat Rev Mol Cell Biol*. 2003;4:397–407.
37. Bomman DM, Mathew S, Alsrube J, et al. Methylation of the E-cadherin gene in bladder neoplasia and in normal urothelial epithelium from elderly individuals. *Am J Pathol*. 2001;159:831–835.
38. Pao MM, Tsutsumi M, Liang G, et al. The endothelin receptor B (EDNRB) promoter displays heterogeneous, site specific methylation patterns in normal and tumor cells. *Hum Mol Genet*. 2001;10:903–910.
39. Newell-Price J, King P, Clark AJ. The CpG island promoter of the human proopiomelanocortin gene is methylated in nonexpressing normal tissue and tumors and represses expression. *Mol Endocrinol*. 2001;15: 338–348.
40. Yagi S, Hirabayashi K, Sato S, et al. DNA methylation profile of tissue-dependent and differentially methylated regions (T-DMRs) in mouse promoter regions demonstrating tissue-specific gene expression. *Genome Res*. 2008;18:1969–1978.
41. Martin GR. Isolation of a pluripotent cell line from early mouse embryos cultured in medium conditioned by teratocarcinoma stem cells. *Proc Natl Acad Sci U S A*. 1981;78:7634–7638.
42. Nagy A, Rossant J, Nagy R, et al. Derivation of completely cell culture-derived mice from early-passage embryonic stem cells. *Proc Natl Acad Sci U S A*. 1993;90:8424–8428.
43. Tanaka S, Kunath T, Hadjantonakis AK, et al. Promotion of trophoblast stem cell proliferation by FGF4. *Science*. 1998;282:2072–2075.
44. Okamoto K, Okazawa H, Okuda A, et al. A novel octamer binding transcription factor is differentially expressed in mouse embryonic cells. *Cell*. 1990;60:461–472.
45. Rosner MH, Vigano MA, Ozato K, et al. A POU-domain transcription factor in early stem cells and germ cells of the mammalian embryo. *Nature*. 1990;345:686–692.
46. Scholer HR, Ruppert S, Suzuki N, et al. New type of POU domain in germ line-specific protein Oct-4. *Nature*. 1990;344:435–439.

47. Sylvester I, Scholer HR. Regulation of the Oct-4 gene by nuclear receptors. *Nucleic Acids Res*. 1994;22:901–911.
48. Nichols J, Zevnik B, Anastassiadis K, et al. Formation of pluripotent stem cells in the mammalian embryo depends on the POU transcription factor Oct4. *Cell*. 1998;95:379–391.
49. Niwa H, Miyazaki J, Smith AG. Quantitative expression of Oct-3/4 defines differentiation, dedifferentiation or self-renewal of ES cells. *Nat Genet*. 2000;24:372–376.
50. Hattori N, Nishino K, Ko YG, et al. Epigenetic control of mouse Oct-4 gene expression in embryonic stem cells and trophoblast stem cells. *J Biol Chem*. 2004;279:17063–17069.
51. Chambers I, Colby D, Robertson M, et al. Functional expression cloning of Nanog, a pluripotency sustaining factor in embryonic stem cells. *Cell*. 2003;113:643–655.
52. Hattori N, Imao Y, Nishino K, et al. Epigenetic regulation of Nanog gene in embryonic stem and trophoblast stem cells. *Genes Cells*. 2007;12:387–396.
53. Do JT, Scholer HR. Cell-cell fusion as a means to establish pluripotency. *Ernst Schering Res Found Workshop*. 2006;60:35–45.
54. Takahashi K, Yamanaka S. Induction of pluripotent stem cells from mouse embryonic and adult fibroblast cultures by defined factors. *Cell*. 2006;126:663–676.
55. Peters TJ, Chapman BM, Wolfe MW, et al. Placental lactogen-I gene activation in differentiating trophoblast cells: extrinsic and intrinsic regulation involving mitogen-activated protein kinase signaling pathways. *J Endocrinol*. 2000;165:443–456.
56. Cho JH, Kimura H, Minami T, et al. DNA methylation regulates placental lactogen I gene expression. *Endocrinology*. 2001;142:3389–3396.
57. Koopman P, Gubbay J, Vivian N, et al. Male development of chromosomally female mice transgenic for Sry. *Nature*. 1991;351:117–121.
58. Nishino K, Hattori N, Tanaka S, et al. DNA methylation-mediated control of Sry gene expression in mouse gonadal development. *J Biol Chem*. 2004;279:22306–22313.
59. Suzuki Y, Tsunoda T, Sese J, et al. Identification and characterization of the potential promoter regions of 1031 kinds of human genes. *Genome Res*. 2001;11:677–684.
60. Ohgane J, Aikawa J, Ogura A, et al. Analysis of CpG islands of trophoblast giant cells by restriction landmark genomic scanning. *Dev Genet*. 1998;22:132–140.
61. Shiota K, Yanagimachi R. Epigenetics by DNA methylation for development of normal and cloned animals. *Differentiation*. 2002;69:162–166.
62. Kremenskoy M, Kremenska Y, Ohgane J, et al. Genome-wide analysis of DNA methylation status of CpG islands in embryoid bodies, teratomas, and fetuses. *Biochem Biophys Res Commun*. 2003;311:884–890.
63. Sakamoto H, Kogo Y, Ohgane J, et al. Sequential changes in genome-wide DNA methylation status during adipocyte differentiation. *Biochem Biophys Res Commun*. 2008;366:360–366.
64. Bjornsson HT, Fallin MD, Feinberg AP. An integrated epigenetic and genetic approach to common human disease. *Trends Genet*. 2004;20:350–358.
65. Iwatani M, Ikegami K, Kremenska Y, et al. Dimethyl sulfoxide has an impact on epigenetic profile in mouse embryoid body. *Stem Cells*. 2006;24:2549–2556.
66. Kannabiran C, Klintworth GK. TGFBI gene mutations in corneal dystrophies. *Hum Mutat*. 2006;27:615–625.
67. Ikeda S, Cunningham LA, Boggess D, et al. Aberrant actin cytoskeleton leads to accelerated proliferation of corneal epithelial cells in mice deficient for destrin (actin depolymerizing factor). *Hum Mol Genet*. 2003;12:1029–1037.
68. Verdoni AM, Aoyama N, Ikeda A, et al. Effect of destrin mutations on the gene expression profile in vivo. *Physiol Genomics*. 2008;34:9–21.
69. Irvine AD, Corden LD, Swensson O, et al. Mutations in cornea-specific keratin K3 or K12 genes cause Meesmann's corneal dystrophy. *Nat Genet*. 1997;16:184–187.
70. Nishida K, Honma Y, Dota A, et al. Isolation and chromosomal localization of a cornea-specific human keratin 12 gene and detection of four mutations in Meesmann corneal epithelial dystrophy. *Am J Hum Genet*. 1997;61:1268–1275.
71. Rodrigues MM, Rajagopalan S, Jones K, et al. Gelsolin immunoreactivity in corneal amyloid, wound healing, and macular and granular dystrophies. *Am J Ophthalmol*. 1993;115:644–652.
72. Bredrup C, Knappskog PM, Majewski J, et al. Congenital stromal dystrophy of the cornea caused by a mutation in the decorin gene. *Invest Ophthalmol Vis Sci*. 2005;46:420–426.
73. Li S, Tiab L, Jiao X, et al. Mutations in PIP5K3 are associated with Francois-Neetens mouchetee fleck corneal dystrophy. *Am J Hum Genet*. 2005;77:54–63.
74. Tsujikawa M, Kurahashi H, Tanaka T, et al. Identification of the gene responsible for gelatinous drop-like corneal dystrophy. *Nat Genet*. 1999;21:420–423.
75. Tasa G, Kals J, Muru K, et al. A novel mutation in the M1S1 gene responsible for gelatinous droplike corneal dystrophy. *Invest Ophthalmol Vis Sci*. 2001;42:2762–2764.
76. Akama TO, Nishida K, Nakayama J, et al. Macular corneal dystrophy type I and type II are caused by distinct mutations in a new sulphotransferase gene. *Nat Genet*. 2000;26:237–241.
77. Li A, Jiao X, Munier FL, et al. Bietti crystalline corneoretinal dystrophy is caused by mutations in the novel gene CYP4V2. *Am J Hum Genet*. 2004;74:817–826.
78. Biswas S, Munier FL, Yardley J, et al. Missense mutations in COL8A2, the gene encoding the alpha2 chain of type VIII collagen, cause two forms of corneal endothelial dystrophy. *Hum Mol Genet*. 2001;10:2415–2423.
79. Gottsch JD, Zhang C, Sundin OH, et al. Fuchs corneal dystrophy: aberrant collagen distribution in an L450W mutant of the COL8A2 gene. *Invest Ophthalmol Vis Sci*. 2005;46:4504–4511.
80. Vithana EN, Morgan P, Sundaresan P, et al. Mutations in sodium-borate cotransporter SLC4A11 cause recessive congenital hereditary endothelial dystrophy (CHED2). *Nat Genet*. 2006;38:755–757.
81. Krafchak CM, Pawar H, Moroi SE, et al. Mutations in TCF8 cause posterior polymorphous corneal dystrophy and ectopic expression of COL4A3 by corneal endothelial cells. *Am J Hum Genet*. 2005;77:694–708.
82. Vincent AL, Patel DV, McGhee CN. Inherited corneal disease: the evolving molecular, genetic and imaging revolution. *Clin Exp Ophthalmol*. 2005;33:303–316.

International Journal of Pharmaceutics 376 (2009) 213–218

Contents lists available at ScienceDirect

International Journal of Pharmaceutics

journal homepage: www.elsevier.com/locate/ijpharm

Note

Effect of gamma-ray irradiation on degradation of di(2-ethylhexyl)phthalate in polyvinyl chloride sheet

Rie Ito[a,*], Naoko Miura[a], Masaru Ushiro[a], Migaku Kawaguchi[b], Hiroko Nakamura[a], Hirofumi Iguchi[c], Jun-ichi Ogino[d], Manabu Oishi[d], Nobuyuki Wakui[a], Yusuke Iwasaki[a], Koichi Saito[a], Hiroyuki Nakazawa[a]

[a] Department of Analytical Chemistry, Faculty of Pharmaceutical Sciences, Hoshi University, 2-4-41 Ebara, Shinagawa-ku, Tokyo 142-8501, Japan
[b] Bio-Medical Standard Section, National Metrology Institute of Japan (NMIJ), National Institute of Advanced Industrial Science and Technology (AIST), Tsukuba Central 3, 1-1-1 Umezono, Tsukuba, Ibaraki 305-8563, Japan
[c] Yokohama Stroke and Brain Center, 1-2-1 Takigashira, Isogo-ku, Yokohama, Kanagawa 235-0012, Japan
[d] Toray Research Center, Inc., 3-3-7 Sonoyama, Otsu, Shiga 520-8567, Japan

ARTICLE INFO

Article history:
Received 29 January 2009
Received in revised form 27 March 2009
Accepted 16 April 2009
Available online 24 April 2009

Keywords:
Liquid chromatography tandem mass spectrometry (LC–MS/MS)
Di(2-ethylhexyl)phthalate (DEHP)
Plasticizer
Gamma ray
Degradation

ABSTRACT

The risk assessment of di(2-ethylhexyl)phthalate (DEHP) migration from polyvinyl chloride (PVC) medical devices is an important issue for patients. The aim of this study was to determine DEHP degradation and migration from PVC sheets. To this end, the method for the simultaneous determination of DEHP and its breakdown products (mono(2-ethylhexyl)phthalate (MEHP) and phthalic acid (PA)) was improved. Their migration levels from 0 to 50 kGy gamma-ray irradiated PVC sheets were determined. DEHP migration level decreased in proportion to the dose of gamma-ray irradiation, while MEHP and PA migration levels increased. The hardness and the elastic modulus of PVC sheets were examined, but no clear relationship between DEHP migration and these parameters was observed.

1. Introduction

Phthalate esters are widely used as industrial plasticizers. In particular, di(2-ethylhexyl)phthalate (DEHP) is used in the production of polyvinyl chloride (PVC) and other plastics to increase flexibility, softness, and stability for specific applications. PVC is one of the most widely used plastic polymers in such medical products as blood containers, blood tubing, and catheters. However, it has been reported that DEHP is easily released from PVC products into food, drugs, and body fluids [Earls et al., 2003; Inoue et al., 2003; Takatori et al., 2004; Ito et al., 2005]. DEHP is considered to exhibit reproductive and developmental toxicity [Lovekamp-Swan and Davis, 2003], carcinogenicity, and testicular toxicity [Tickner et al., 2001; Yakubovich and Vienken, 2000; Hill et al., 2001]. Some phthalates including DEHP are said to exhibit toxic effects, including antiandrogenic effects during reproductive system development and normal sperm production in male rat [Poon et al., 1997; Lamb et al., 1987; Tyl et al., 1988], and the decrease in blood 17β-estradiol level in female rat [Davis et al., 1994]. In addition, recent studies have shown that certain phthalate exposure levels in pregnant women are associated with the reproductive health of male infants [Latini et al., 2003; Swan et al., 2005; Marsee et al., 2006]. In Japan, The Ministry of Health, Labour and Welfare (2000) has set the tolerable daily intake (TDI) of DEHP at 40–140 μg kg^{-1} day^{-1} and has regulated the use of DEHP as plasticizer in the manufacture of infant toys.

In our previous studies, we observed that not only DEHP but also mono(2-ethylhexyl)phthalate (MEHP) and phthalic acid (PA) migrated from PVC medical devices into simulated pharmaceuticals even without enzymatic hydrolysis [Ito et al., 2005, 2006, 2008]. DEHP migration was suppressed by the sterilization process, particularly gamma-ray sterilization [Ito et al., 2006]. In contrast, MEHP migration from gamma-ray sterilized PVC medical device was increased dramatically [Ito et al., 2006, 2008]. Since MEHP is thought to be even more toxic than DEHP, the formation of MEHP as a breakdown product of DEHP is a critical problem.

In this study, DEHP, MEHP, and PA migration levels were determined to confirm the effect of gamma-ray irradiation on the degradation of DEHP. Commercially available PVC medical devices are generally subjected to 20–25 kGy gamma-ray sterilization. Therefore, PVC sheets used in the manufacture of blood bags were irradiated with 1–50 kGy gamma rays. No sterilization process

* Corresponding author. Tel.: +81 3 5498 5765; fax: +81 3 5498 5765.
E-mail address: rie-ito@hoshi.ac.jp (R. Ito).

0378-5173/$ – see front matter © 2009 Elsevier B.V. All rights reserved.
doi:10.1016/j.ijpharm.2009.04.019

was performed on the control sample (non-irradiated gamma ray: 0 kGy). DEHP, MEHP, and PA migration levels were examined in relation to the dose of gamma rays. Moreover, the hardness and the elastic modulus of irradiated PVC sheet were examined because surface processing, an example of which is polyethylene glycol grafting, is known to suppress DEHP migration [Lakshmi and Jayakrishnan, 1998]. Then, the effect of gamma-ray irradiation on the PVC surface was studied to understand the relationship between DEHP, MEHP, and PA migration levels and the hardness and the elastic modulus of irradiated PVC sheets.

2. Materials and methods

2.1. Chemicals and materials

Environmental analytical grade DEHP and DEHP-d_4 were purchased from Kanto Chemical Co. Inc. (Tokyo, Japan). MEHP and MEHP-d_4 were purchased from Hayashi Pure Chemical Industries (Osaka, Japan). PA and PA-d_4 were purchased from CDN Isotope Central Chemicals Co. Inc. (Tokyo, Japan). Phthalic acid esters, analytical grade acetonitrile, and acetone were used in the experiments. Analytical grade formic acid was obtained from Wako Pure Chemical Industries Ltd. (Osaka, Japan). The water purification system used was a Milli-Q gradient A 10 with an EDS polisher (Millipore, Bedford, MA, USA).

The test material was PVC sheet subjected to gamma-ray irradiation (^{60}Co; 1, 5, 10, 25, 50 kGy). Commercial medical devices were irradiated with approximately 25 kGy gamma rays for sterilization. The control sample was not irradiated with gamma rays. The PVC sheets were kindly supplied by the manufacturer.

The extraction solvents were 5% glucose solution for injection (Otsuka Pharmaceuticals Co., Tokyo, Japan), polyoxyethylated hydrogenated castor oil 60 (HCO-60) (Wako Pure Chemical Industries Ltd., Osaka, Japan), and purified water.

2.2. Instrumentation and LC–MS/MS conditions

A Series 1100 liquid chromatograph from Agilent Technologies (USA) was coupled to an API 4000™ (Applied Biosystems Japan, Tokyo, Japan) equipped with a Turbo Ionspray™ ionization source. Mass spectrometry data were processed with Analyst 1.3.2 software. An Inertsil-Ph3 column (50 mm × 2.1 mm, 5 μm particle size) from GL Sciences was used for separation.

After 5 μL of the sample was injected with an auto-sampler, it was loaded onto the analytical column by introducing the mobile phase at the flow rate of 0.2 ml min^{-1}. The auto-sampler was maintained at 4 °C to keep the sample cool. Acetonitrile (mobile phase A) and 0.05% formic acid in water (mobile phase B) were used. Separation was carried out with the following profile: mobile phase A/B was 15/85 (0–4 min) → 90/10 (4.01–15 min for elution) → 15/85 (15.01–25 min for equilibration) (v/v). The column oven was maintained at 40 °C for LC.

The working parameters for turbo ionspray ionization MS/MS were as follows: curtain gas, 20 psi (DEHP and DEHP-d_4 for the positive ion mode) and 20 psi (MEHP, PA, and their internal standards for the negative ion mode); nebulizer gas (N_2) pressure, 80 psi for the positive ion mode and 80 psi for the negative ion mode; and turbo ionspray gas (N_2) pressure, 60 psi for the positive ion mode and 60 psi for the negative ion mode. Ion source temperature was maintained at 650 °C and turbo ionspray voltages for the positive ion mode (DEHP, DEHP-d_4) and the negative ion mode (MEHP, PA, and their internal standards) were 5000 and −4500 V, respectively. Declustering potentials of DEHP, MEHP, and PA were 61 V, −60 V, and −35 V, respectively. DEHP and DEHP-d_4 were monitored in the positive ion mode, whereas MEHP, PA, and their internal standards were monitored in the negative ion mode. The combinations of precursor ion and product ions were as follows: DEHP (precursor ion → product ion, m/z 391 → 149), DEHP-d_4 (m/z 395 → 153), MEHP (m/z 277 → 134), MEHP-d_4 (m/z 281 → 138), PA (m/z 165 → 121), and PA-d_4 (m/z 169 → 125). The collision gas (N_2) pressure was set at 4 units for both positive and negative ion modes. These conditions were modified from those of our previous paper [Ito et al., 2008].

2.3. Effect of gamma-ray irradiation on migration test

The migration of DEHP, MEHP, and PA from PVC sheet (1 cm × 3 cm) into 5 ml of each extraction solvent was examined. 5% glucose solution, HCO-60, and purified water were used as extraction solvent. They also served as simulated pharmaceuticals. HCO-60 is a surfactant that is involved in the migration of DEHP into such drugs as Prograf®. The extent of DEHP migration was dependent on the concentration of HCO-60 [Hanawa et al., 2003]. In this study, 2 mg ml^{-1} HCO-60 was prepared for the migration test. The concentration of HCO-60 was set with reference to its content in commercial pharmaceuticals as surfactant. The samples were kept in test tubes and extraction was carried out by shaking at 37 °C for 1 h. An aliquot (1 ml) of the extract was pipetted into another test tube and DEHP-d_4, MEHP-d_4, and PA-d_4 were added. Then, the sample solution was appropriately diluted prior to LC–MS/MS analysis.

2.4. Instrumentation and conditions for indentation measurement

The hardness and the elastic modulus of non-irradiated (0 kGy) and irradiated PVC sheets (25 and 50 kGy) were measured by a depth-sensing nanoindentation technique with Nano indenter XP (MTS Systems Co., Oak Ridge, TN, USA). PVC sheets were indented with a Berkovich diamond tip to a maximum depth of 55 μm at room temperature (23 ± 1 °C). The indentation load–displacement behavior of gamma-ray irradiated PVC sheets was tested in the continuous stiffness measurement mode. As shown in Fig. 1, load–displacement curves were obtained to determine the

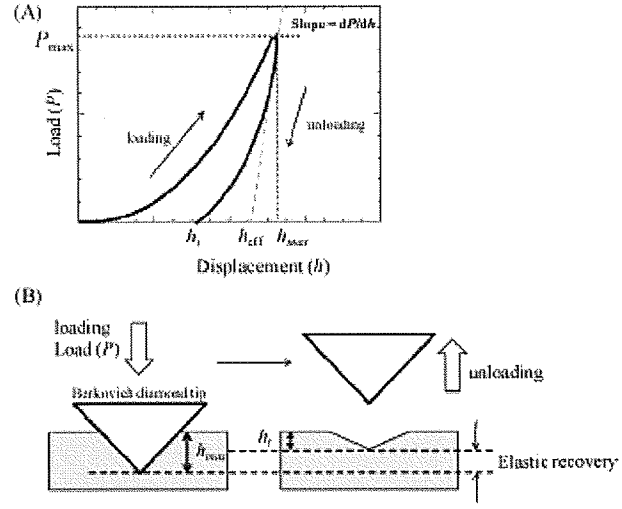

Fig. 1. Determination of hardness and the elastic modulus. (A) Typical load versus displacement curve. (B) Schematic diagram of indentation measurement.

Table 1
Figures of merit of LC–MS/MS method for determination of DEHP, MEHP, and PA.

	Range (ng ml^{-1})	Spiked conc. (ng ml^{-1})	Purified water		5% glucose		HCO-60	
	(r)		Recovery (%)	RSD (%)	Recovery (%)	RSD (%)	Recovery (%)	RSD (%)
DEHP	20–1000	100	97.5	6.2	97.2	4.4	98.5	1.8
	(0.998)	500	97.5	1.8	99.9	0.9	94.5	1.2
MEHP	2–1000	100	102	2.4	105	5.2	105	2.5
	(0.999)	500	98.2	3.1	101	1.8	104	3.9
PA	5–1000	100	97.0	7.8	90.4	7.0	107	3.4
	(0.999)	500	102	1.8	102	2.1	104	1.4

r: correlation coefficient; RSD: relative standard deviation ($n = 3$).

hardness (H) and the elastic modulus (E) of the sheets. Theoretical elastic modulus and theoretical hardness were calculated as follows:

$$E \approx \frac{\sqrt{\pi}}{2\beta}\frac{1}{\sqrt{kh_{gf}^2}}\frac{dP}{dh} \quad \text{and} \quad H = \frac{P_{max}}{kh_{gf}^2}$$

where β and k are constants. When the Berkovich diamond tip was used, $k = 24.56$ and $\beta = 1.034$.

Hardness and elastic modulus were calculated by multiplying modification coefficient (η) by the theoretical hardness and the theoretical elastic modulus. In addition, modification coefficient was confirmed with a load–displacement curve obtained from a calibration experiment using silica.

3. Results and discussion

3.1. Optimization of the LC–MS/MS method

In the scan mode, DEHP, MEHP, and PA were monitored at m/z 391, 277, and 165, which were assigned to $[M+H]^+$, $[M-H]^-$, and $[M-H]^-$, respectively. Moreover, in the product ion MS/MS measurement, selective reaction monitoring ions (SRMs) of DEHP, DEHP-d_4, MEHP, MEHP-d_4, PA, and PA-d_4 were set depending on their precursor ions. When the auto-sampler was maintained at room temperature, the peak shape was not good. However, when the auto-sampler was maintained at 4 °C to keep the sample cool, a reproducible peak area was obtained. In addition, the sample solution was acidified (1%) to improve separation. No interference from peaks of the other compounds present in the extraction solvents was noted.

3.2. Figures of merit of LC–MS/MS analysis for determination of DEHP, MEHP, and PA

In the proposed method, determination was achieved by stable isotope dilution analyses. The limits of detection (LODs) of DEHP, MEHP, and PA subjected to LC–MS/MS analysis were 5, 0.5, and 1 ng ml^{-1}, respectively, and the signal-to-noise (S/N) ratio was 3. In addition, the limits of quantification (LOQs) of DEHP, MEHP, and PA when S/N > 10 were 20, 2, and 5 ng ml^{-1}, respectively. The method showed good linearity and the correlation coefficients (r) were higher than 0.998 for all the analytes. The figures of merit of the present method are summarized in Table 1. Sensitivity and accuracy were sufficient for the determination of DEHP, MEHP, and PA migration levels from PVC sheets.

The recovery and precision of the method were assessed by replicate analyses ($n = 3$) of each solvent spiked at 100 and 500 ng ml^{-1} levels. Non-spiked and spiked samples were subjected to LC–MS/MS analysis. Recovery was calculated by subtracting the results for the non-spiked samples from those for the spiked samples. The results were obtained by using calibration curves acquired from standard solutions containing the surrogate compounds. The recovery and precision were 97.0–102% (relative standard deviation—RSD: 1.8–7.8%), 90.4–105% (RSD: 0.9–7.0%), and 94.5–107% (RSD: 1.2–3.9%) for purified water, 5% glucose solution, and HCO-60, respectively (Table 1). Therefore, the method enables the precise determination of standards and may be applicable to the determination of DEHP, MEHP, and PA in pharmaceutical solutions containing HCO-60 as surfactant.

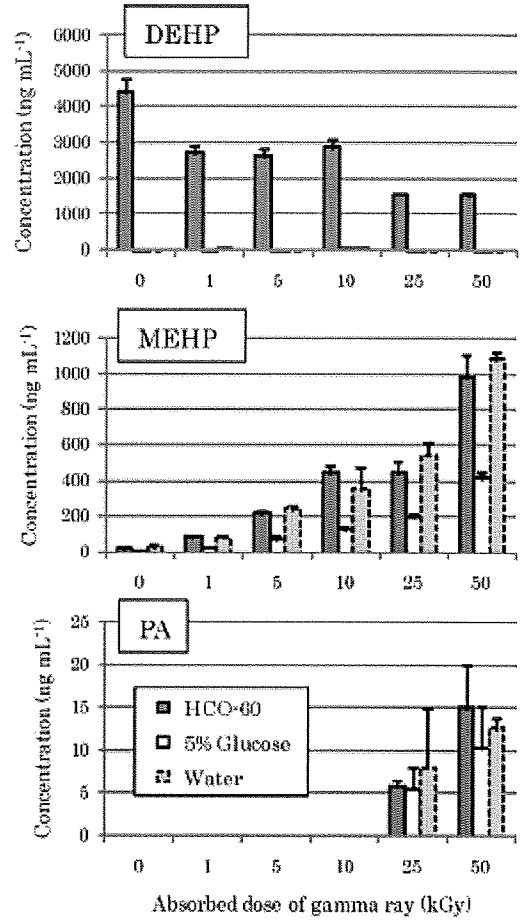

Fig. 2. Concentrations of DEHP, MEHP, and PA that migrated from gamma-ray irradiated PVC sheet. Extraction solvents HCO-60, 5% glucose solution, and water are represented by dark columns with a solid line, white columns with a solid line, and gray columns with a dotted line, respectively.

3.3. Effect of gamma-ray irradiation on DEHP degradation

DEHP, MEHP, and PA migration levels from gamma-ray irradiated PVC sheets are shown in Fig. 2. Similar to that reported in another paper [Ito et al., 2006], DEHP migration was marked when HCO-60 was used as the extraction solvent. DEHP, MEHP, and PA migration from PVC sheets was influenced by gamma-ray irradiation. The higher the dose of irradiated gamma rays, the lower DEHP migration level from the PVC sheets. In contrast, MEHP migration from the irradiated PVC sheets was dependent on the dose of gamma-ray irradiation. In the case of PVC sheets subjected to 1 and 5 kGy gamma-ray irradiation and non-irradiated (0 kGy), no PA was detected (below LOD). In PVC sheets exposed to 10 kGy gamma-ray irradiation, trace level of PA was detected (between LOD and LOQ). PA was clearly detected when the gamma-ray irradiation exceeded 25 kGy. The amount of PA that migrated from the 50 kGy gamma-ray irradiated PVC sheet was higher than that from the 25 kGy irradiated one. Therefore, PA migration from the irradiated PVC sheet was thought to be dependent on the gamma-ray irradiation dose applied to the PVC sheet.

It should be noted that the molar concentration of DEHP that was decreased upon gamma-ray irradiation was not equal to the total molar concentration of MEHP and PA that was increased upon gamma-ray irradiation; however, taking into consideration the fact that MEHP migration level was well correlated with the dose of gamma-ray irradiation, we can say that MEHP and PA were formed from the breakdown of DEHP by gamma-ray irradiation. Moreover, there is a possibility that other factors were involved in the migration of these compounds.

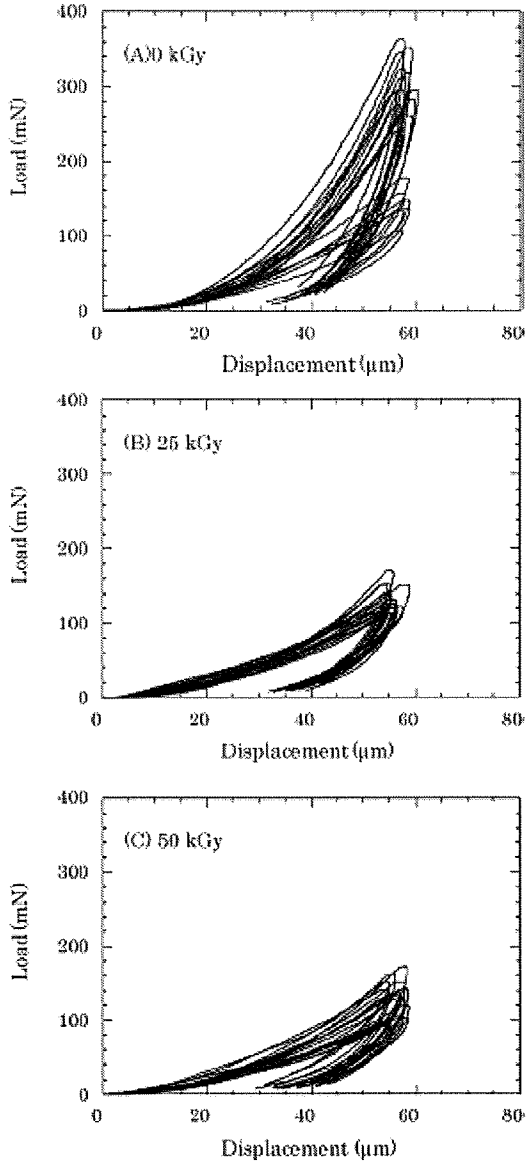

Fig. 3. Load–displacement curves for 0, 25, and 50 kGy gamma-ray irradiated PVC sheets. These load–displacement curves were obtained from (A) 0 kGy gamma-ray irradiated PVC sheet, (B) 25 kGy gamma-ray irradiated PVC sheet, and (C) 50 kGy gamma-ray irradiated PVC sheet.

3.4. Indentation measurement of gamma-ray irradiated PVC sheets

The load–displacement curves for non-irradiated (0 kGy) and irradiated (25 and 50 kGy gamma ray) PVC sheets are shown in Fig. 3. Although the load–displacement curves were scattered widely, replicate studies ($n = 20$) were conducted to determine the average behavior. It was thought that the contact state between the Berkovich diamond tip and the PVC sheet could not be kept in the same state because of the rough surface of the PVC sheet (Fig. 4). From the load–displacement curves, Young's modulus versus depth plots (Fig. 5A) and hardness versus depth plots (Fig. 5B) were obtained. As shown in Fig. 5, the correlation between hardness and depth or between elastic modulus and depth was observed. In particular, below 20 μm depth, a difference was observed between non-irradiated sample (0 kGy) and irradiated samples (25 and 50 kGy). However, it is thought that the data were influenced by the rough surface of the PVC sheet when monitoring was carried out at small depths. Similarly, when monitoring was carried out at large depths (≥40 μm), the data were influenced by the rough back surface as the PVC sheet itself was approximately 400 μm thick. The elastic modulus and the hardness at 1, 5, 10, and 20 μm depth from the surface are shown in Table 2. In calculating the elastic modulus, the Poisson ratio was empirically assumed to be 0.3. As a result, the elastic modulus of gamma-ray irradiated PVC sheet was higher than that of the non-irradiated sample. Surface PVC chains might be cross-linked or broken by gamma-ray irradiation [Mendizabal et al., 1996; Baccaro et al., 2003; Silva et al., 2008] and might be influenced by the migration of DEHP, MEHP, and PA.

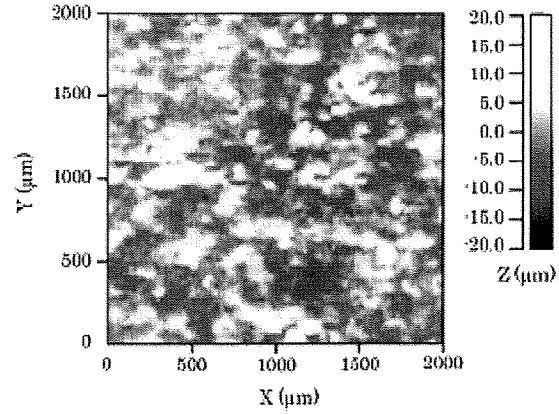

Fig. 4. 3D surface topography of non-irradiated PVC sheet. KLA-Tencor P-15 contact stylus profiler was used to measure the surface roughness of a sample PVC sheet.

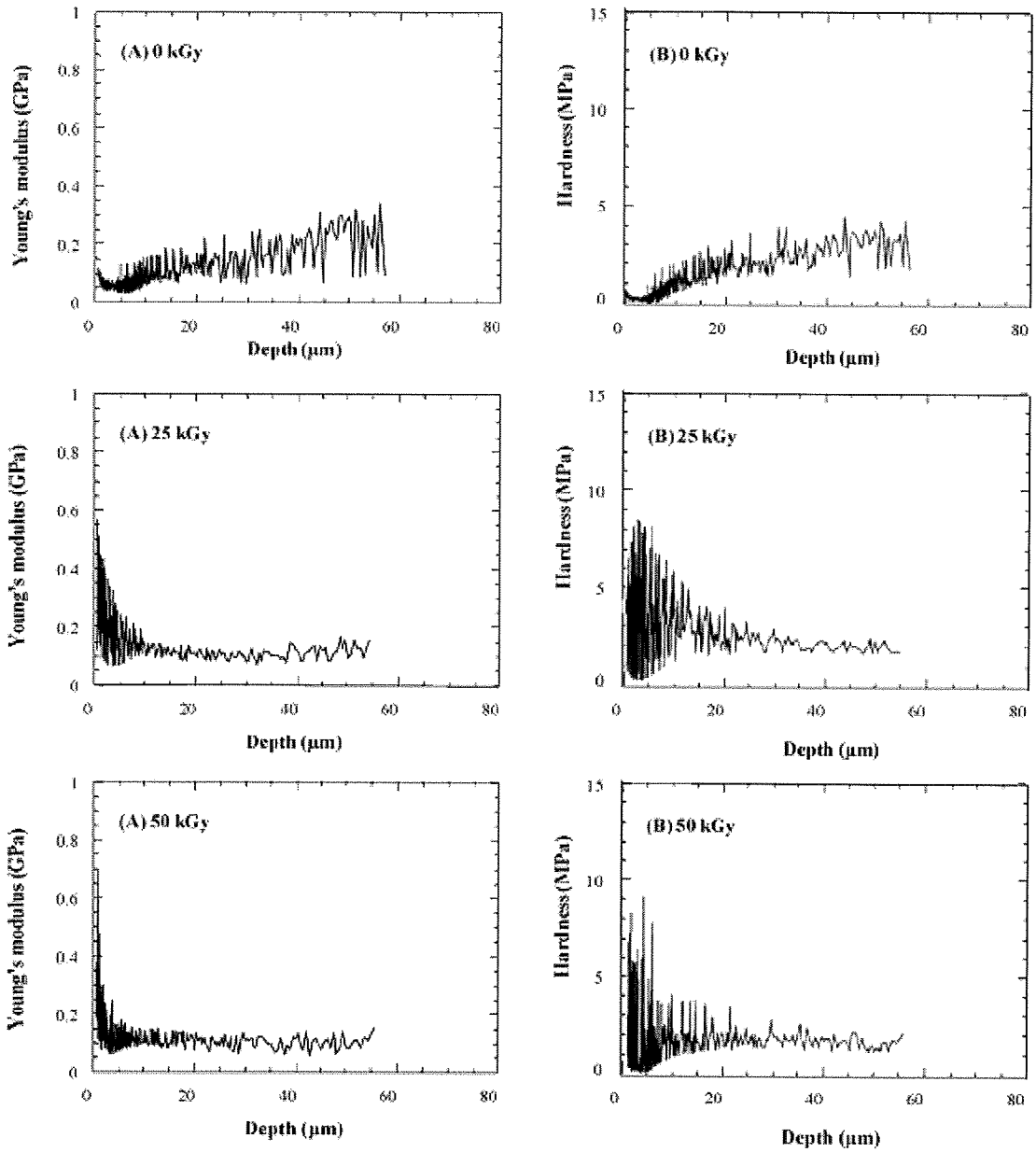

Fig. 5. Young's modulus versus depth (A) and hardness versus depth (B) diagrams. Top panels show data for non-irradiated PVC sheet (0 kGy). Middle panels show data for 25 kGy irradiated PVC sheet. Bottom panels show data for 50 kGy irradiated PVC sheet.

Table 2
Elastic modulus and hardness.

Depth (μm)	Control		25 kGy		50 kGy	
	Elastic modulus (MPa)	Hardness (MPa)	Elastic modulus (MPa)	Hardness (MPa)	Elastic modulus (MPa)	Hardness (MPa)
1	80 ± 17	0.42 ± 0.11	330 ± 120	2.9 ± 1.9	240 ± 140	2.0 ± 2.3
5	59 ± 22	0.37 ± 0.22	180 ± 50	4.3 ± 2.3	130 ± 37	2.3 ± 2.3
10	93 ± 35	1.1 ± 0.45	130 ± 21	3.6 ± 1.5	120 ± 19	2.2 ± 1.2
20	130 ± 32	2.0 ± 0.56	100 ± 14	2.5 ± 0.7	100 ± 19	2.1 ± 0.6

Poisson ratio of sample was assumed to be 0.3 when elastic modulus was calculated.

4. Conclusion

MEHP was formed from DEHP degradation depending on the dose of gamma-ray irradiation. Moreover, DEHP migration depended on its decomposition to MEHP or PA. The cross-linking or scission of surface PVC chains might be influenced by DEHP, MEHP, and PA migration from the PVC sheet. However, it is an undeniable fact that MEHP migration level increased with increasing dose of irradiated gamma rays. MEHP is thought to be more toxic than DEHP. Therefore, MEHP exposure should be taken into consideration in the assessment of DEHP exposure in high-risk patients. The gamma-ray sterilization process uses at least 20–25 kGy gamma rays as sterilization dose, and it is possible that even higher doses are used to sterilize medical devices. In the present paper,

apparent high correlations between hardness or elastic modulus of PVC surface and migration levels of DEHP, MEHP, or PA were not observed. However, any relationship between plasticizer migration and gamma-ray effect on the PVC surface is undeniable possibility. We should further study in greater detail the relationship between plasticizer migration and gamma-ray effect on the PVC surface.

Acknowledgements

This study was partly supported by Health Sciences Research Grants from the Ministry of Health, Labour and Welfare, Japan; the Science/Technology Frontier Research Base of the Ministry of Education, Culture, Sports, Science and Technology, Japan; and a Grant-in-Aid for Young Scientists (B) from the Ministry of Education, Culture, Sports, Science and Technology, Japan. These PVC sheets which were not irradiated by gamma ray were kindly supplied by Terumo Corporation (Tokyo, Japan). Gamma-ray irradiation of PVC sheet was accomplished, courtesy of the Japan Radioisotope Association. We would like to thank Dr. Hironiwa T., who belongs to the Japan Radioisotope Association, for an advice of gamma-ray expert. We would like to thank Mr. Takeda M., who belongs to Toray Research Center, for indentation measurement and for technical review of the manuscript.

References

Baccaro, S., Brunella, V., Cecilia, A., Costa, L., 2003. γ irradiation of poly(vinyl chloride) for medical applications. Nucl. Instrum. Methods Phys. Res. 208, 195–198.

Davis, B.J., Maronpot, R.R., Heindel, J.J., 1994. Di-(2-ethylhexyl)phthalate suppresses estradiol and ovulation in cycling rats. Toxicol. Appl. Pharmacol. 128, 216–223.

Earls, A.O., Axford, I.P., Braybrook, J.H., 2003. Gas chromatography–mass spectrometry determination of the migration of phthalate plasticisers from polyvinyl chloride toys and childcare articles. J. Chromatogr. A 983, 237–246.

Hanawa, T., Endoh, N., Kazuno, F., Suzuki, M., Kobayashi, D., Tanaka, M., Kawano, K., Morimoto, Y., Nakajima, S., Oguchi, T., 2003. Investigation of the release behavior of diethylhexyl phthalate from polyvinyl chloride tubing for intravenous administration based on HCO60. Int. J. Pharm. 267, 141–149.

Hill, S., Shaw, B., Wu, A., 2001. The clinical effects of plasticizers, antioxidants, and other contaminants in medical polyvinylchloride tubing during respiratory and non-respiratory exposure. Clin. Chim. Acta 304, 1–8.

Inoue, K., Kawaguchi, M., Okada, F., Yoshimura, Y., Nakazawa, H., 2003. Column-switching high-performance liquid chromatography electrospray mass spectrometry coupled with on-line of extraction for the determination of mono- and di-(2-ethylhexyl)phthalate in blood samples. Anal. Bioanal. Chem. 375, 527–533.

Ito, R., Miura, N., Kawaguchi, M., Ushiro, M., Iguchi, H., Iwasaki, Y., Saito, K., Nakazawa, H., 2008. Simultaneous determination of di(2-ethylhexyl)phthalate, mono(2-ethylhexyl)phthalate, and phthalic acid migrating from gamma-ray irradiated polyvinyl chloride sheet by liquid chromatography–tandem mass spectrometry. J. Liq. Chromatogr. Relat. Technol. 31, 198–209.

Ito, R., Seshimo, F., Miura, N., Kawaguchi, M., Saito, K., Nakazawa, H., 2005. High-throughput determination of mono- and di(2-ethylhexyl)phthalate migration from PVC tubing to drugs using liquid chromatography–tandem mass spectrometry. J. Pharm. Biomed. Anal. 39, 1036–1041.

Ito, R., Seshimo, F., Miura, N., Kawaguchi, M., Saito, K., Nakazawa, H., 2006. Effect of sterilization process on the formation of mono(2-ethylhexyl)phthalate from di(2-ethylhexyl)phthalate. J. Pharm. Biomed. Anal. 41, 455–460.

Lakshmi, S., Jayakrishnan, A., 1998. Migration resistant, blood-compatible plasticized polyvinyl chloride for medical and related applications. Artif. Organs 22, 222–229.

Lamb, J.C., Chapin, R.E., Teague, J., Lawton, A.D., Reel, J.R., 1987. Reproductive effects of four phthalic acid esters in the mouse. Toxicol. Appl. Pharmacol. 88, 255–269.

Latini, G., Defelice, C., Presta, G., Del Vecchio, A., Paris, I., Ruggieri, F., Mazzeo, P., 2003. In utero exposure to di-(2-ethylhexyl)phthalate and duration of human pregnancy. Environ. Health Perspect. 111, 1783–1785.

Lovekamp-Swan, T., Davis, B.J., 2003. Mechanisms of phthalate ester toxicity in the female reproductive system. Environ. Health Perspect. 111, 139–145.

Marsee, K., Woodruff, T.J., Axelrad, D.A., Calafat, A.M., Swan, S.H., 2006. Estimated daily phthalate exposures in a population of mothers of male infants exhibiting reduced anogenital distance. Environ. Health Perspect. 114, 805–809.

Mendizabal, E., Cruz, L., Jasso, C.F., Burillo, G., Dakin, V.I., 1996. Radiation crosslinking of highly plasticized PVC. Radiat. Phys. Chem. 47, 305–309.

Poon, R., Lecavalier, P., Mueller, R., Valli, V.E., Procter, B.G., Chu, I., 1997. Subchronic oral toxicity of di-n-octyl phthalate and di(2-ethylhexyl)phthalate in the rat. Food Chem. Toxicol. 35, 225–239.

da Silva, F.F. da, Aquino, K.A. da S., da Araújo, E.S., 2008. Effects of gamma irradiation on poly(vinyl chloride)/polystyrene blends: investigation of radiolytic stabilization and miscibility of the mixture. Polym. Degrad. Stab. 93, 2199–2203.

Swan, S.H., Main, K.M., Liu, F., Stewart, S.L., Kruse, R.L., Calafat, A.M., Mao, C.S., Redmon, J.B., Ternand, C.L., Sullivan, S., Teague, J.L., 2005. Decrease in anogenital distance among male infants with prenatal phthalate exposure. Environ. Health Perspect. 113, 1056–1061.

Takatori, S., Kitagawa, Y., Kitagawa, M., Nakazawa, H., Hori, S., 2004. Determination of di(2-ethylhexyl)phthalate and mono(2-ethylhexyl)phthalate in human serum using liquid chromatography–tandem mass spectrometry. J. Chromatogr. B 804, 397–401.

The Ministry of Health, Labour and Welfare, 2000. Website: http://www1.mhlw.go.jp/shingi/s0006/txt/s0614-1_13.txt (in Japanese).

Tickner, J.A., Schettler, T., Guidotti, T., McCally, M., Rossi, M., 2001. Health risks posed by use of di-2-ethylhexyl phthalate (DEHP) in PVC medical devices: a critical review. Am. J. Ind. Med. 39, 100–111.

Tyl, R.W., Price, C.J., Marr, M.C., Kimmel, C.A., 1988. Developmental toxicity evaluation of dietary di(2-ethylhexyl)phthalate in Fischer 344 rats and CD-1 mice. Fundam. Appl. Toxicol. 10, 395–412.

Yakubovich, M., Vienken, J., 2000. Is there a need for plasticizer-free biomaterials in dialysis therapy? Med. Device Technol. 11, 18–21.

Bull Environ Contam Toxicol (2010) 84:212–216
DOI 10.1007/s00128-009-9919-x

Determination of Phthalates in Diet and Bedding for Experimental Animals Using Gas Chromatography-Mass Spectrometry

Fumio Kondo · Masanao Okumura · Hisao Oka · Hiroyuki Nakazawa · Shun-ichiro Izumi · Tsunehisa Makino

Received: 23 June 2009 / Accepted: 18 November 2009 / Published online: 1 December 2009

Abstract We have developed a gas chromatography–mass spectrometry method to measure five phthalates (dibutyl phthalate, butylbenzyl phthalate, di-2-ethylhexyl phthalate, diisooctyl phthalate, and diisononyl phthalate) in diets and beddings for experimental animals. The recoveries from diets and beddings spiked with five phthalates were 98.8%–148% with coefficients of variation of 0.4%–7.8% for diets and 94.7%–146% with coefficients of variation of 1.0%–5.0% for beddings. We analyzed commercial animal diets and beddings, and found that the levels of phthalates varied from sample to sample; the concentrations of five phthalates were 141–1,410 ng/g for diets and 20.5–7,560 ng/g for beddings.

Keywords Phthalates · Animal diets · Beddings · Gas chromatography-mass spectrometry

F. Kondo · M. Okumura · H. Oka
Department of Toxicology, Aichi Prefectural Institute of Public Health, 7-6 Nagare, Tsuji-machi, Kita-ku, Nagoya 462-8576, Japan

H. Nakazawa
Department of Analytical Chemistry, Hoshi University, 2-4-41 Ebara, Shinagawa-ku, Tokyo 142-8501, Japan

S. Izumi · T. Makino
Department of Obstetrics and Gynecology, School of Medicine, Tokai University, Bohseidai, Isehara 25-1193, Japan

F. Kondo (✉)
Department of Pharmacology, School of Medicine, Aichi Medical University, Nagakute, Aichi 480-1195, Japan
e-mail: fumio@ipc-tokai.or.jp

Phthalates are used as additives, as solvents, and as plasticizers in many consumer products. The widespread manufacture, use, and disposal of phthalates have caused ubiquitous environmental pollution and humans are regularly exposed to phthalates (Blount et al. 2000; Silva et al. 2004; Kato et al. 2005). Certain phthalates, such as dibutyl phthalate (DBP), butylbenzyl phthalate (BBzP), di-2-ethylhexyl phthalate (DEHP) and diisononyl phthalate (DINP), have been shown to disrupt development of the reproductive tract in male rodents in an antiandrogenic manner (Parks et al. 2000). Concern has been raised about phthalates in relation to effects on the reproductive tract in adult males and the development of male offspring in humans (Duty et al. 2003; Swan et al. 2005).

When animal toxicology of phthalates is studied, it is necessary to take into account the exposure from the diet and the experimental environment. Since the complete exclusion of phthalate may well be impossible, the precise concentration of phthalates in the diet, bedding and water used for feeding, the air in the experimental animal room, etc. could be important information needed to attain reliability of animal experiments. To our knowledge, no study of phthalate contamination of diets or experimental environments has been reported.

We have developed a gas chromatography-mass spectrometry (GC-MS) method to determine five commonly used phthalates (DBP, DEHP, BBzP, DINP and diisooctyl phthalate (DIOP)) in animal diets and beddings. The method was used for the analysis of commercial diets and beddings for experimental animals. Additionally, in order to investigate the other causes of rodent exposure to phthalates in feeding conditions, we analyzed water supplied to the animals, and samples of air taken from the animal room.

Materials and Methods

DBP, DEHP, BBzP, DIOP, DINP, DBP-3,4,5,6-d_4, DEHP-3,4,5,6-d_4, BBzP-3,4,5,6-d_4, and DOP-3,4,5,6-d_4 were purchased from Kanto Chemical (Tokyo, Japan). DNP-3,4,5,6-d_4 was purchased from Hayashi Pure Chemicals (Osaka, Japan). Phthalic acid esters and analytical grade acetonitrile, hexane, acetone and sodium chloride were purchased from Kanto Chemical. Pesticide analysis grade sodium sulfate was purchased from Wako Pure Chemical Industries (Osaka, Japan). Bondesil-PSA (40 μm pore size) was purchased from Varian (CA, USA). Florisil® PR was purchased from Wako Pure Chemical Industries. The water used for extraction was prepared by washing distilled water with hexane.

Rodent diets were obtained from CLEA Japan Inc. (Tokyo, Japan), Oriental Yeast Co. Ltd (Tokyo, Japan), and Nihon Nosan Kogyo Co. Ltd (Tokyo, Japan). Animal beddings were obtained from Charles River Laboratories Japan Inc. (Yokohama, Japan), Japan SLC, Inc. (Hamamatsu, Japan), CLEA Japan Inc., and Oriental Yeast Co. Ltd.

Since some of phthalates analyzed in this study are very abundant and contamination is practically unavoidable (Takatori et al. 2004), the contamination preventive measures were given as follows. No plastic apparatus was used in these experiments. The reagents and solvents were used just after opening or were not left for a long time after opening. All of the experimental apparatus, including glassware and spatulas, were washed carefully with acetone and hexane, and then heated at 200°C for 2 h to remove any phthalates. They were washed with acetone and hexane just before use. Sodium chloride, sodium sulfate and Florisil® PR were heated at 200°C for 2 h. Before starting the experiment, we took various precautionary measures, such as shortening fingernails, washing hands well with soap, covering the laboratory bench with aluminum foil, etc. A blank analysis was carried out before sample analysis in each batch. The evaporator was cleaned before use by evaporating 10 mL of acetone.

A Florisil and Bondesil-PSA column was prepared by packing Florisil (1 g), Bondesil-PSA (0.5 g) and sodium sulfate (2 g) in turn into a glass syringe (15 mm × 110 mm). The column was washed with acetone (10 mL) and hexane (10 mL) before use.

Stock solutions of native standards (DBP, DEHP, BBzP, DIOP, DINP) and isotope-labeled internal standards (DBP-3,4,5,6-d_4, DEHP-3,4,5,6-d_4, BBzP-3,4,5,6-d_4, DOP-3,4,5,6-d_4, DNP-3,4,5,6-d_4) were prepared in acetonitrile and stored at −20°C in Teflon-capped glass bottles until use. They were mixed at the desired ratio and serially diluted for calibration curves. The peak area ratio of analyte to isotope-labeled internal standard was used for quantification. Reproducible calibration curves for five phthalates were obtained with correlation coefficients greater than 0.999 (known concentration vs analyte/internal standard). They were linear over the range of 10–1,000 ng/mL for DBP, BBzP and DEHP and 50–1,000 ng/mL for DIOP and DINP.

The present method for analysis of phthalates in diets is a modification of that described by Tsumura et al. (2001). A sample of the diet (5 g) was weighed into a centrifuge tube, followed by water (5 mL) and acetonitrile (20 mL), and spiked with isotopically labeled internal standards (4 μg/mL, 25 μL). The sample was homogenized for 1 min using a homogenizer (Physcotron, Microtec Co. ltd), and then centrifuged at 3,000 rpm for 5 min. The acetonitrile layer was collected, and the residual homogenate was extracted again with 75% acetonitrile in water (20 mL). The acetonitrile layers were combined, sodium chloride (1.5 g) was added, and the mixture was shaken vigorously for 5 min. The acetonitrile layer was collected, hexane saturated with acetonitrile (4 mL) was added, and the mixture was shaken vigorously for 5 min. The acetonitrile layer was evaporated to dryness under reduced pressure at 35°C. The residue was dissolved in water (2 mL) and hexane (5 mL) and the mixture was shaken vigorously for 30 s. The solution was centrifuged at 3,000 rpm for 5 min, and the hexane layer was removed and saved. Hexane (3 mL) was added to the water layer, and extracted as described above. The hexane layers were combined and loaded onto a Florisil and Bondesil-PSA dual layer column, which was preconditioned with acetone (10 mL) and hexane (10 mL). After washing the column with hexane (3 mL), phthalates were eluted with 5% acetone in hexane (10 mL). The eluate was evaporated to dryness under reduced pressure at 35°C, and then dissolved in hexane (1 mL). An aliquot of each sample (2 μL) was injected into a GC-MS system.

The present method for analysis of phthalates in bedding is a modification of that described by Tsumura et al. (2001). A sample of bedding for experimental animals (5 g) was weighed into a centrifuge tube followed by acetone (40 mL), and spiked with isotopically labeled internal standards (4 μg/mL, 25 μL). The sample was left for 1 h and then shaken vigorously for 10 min. The solution was evaporated to dryness under reduced pressure at 35°C. The residue was treated as described for diets.

Analysis of phthalates in water was carried out as described (Glick 1998). Water (30 mL) from a tap in the experimental animal room was weighed into a centrifuge tube followed by hexane (10 mL), spiked with isotopically labeled internal standards (4 μg/mL, 25 μL), then shaken vigorously for 10 min. The hexane layer was evaporated to dryness under reduced pressure at 35°C. The residue was dissolved in hexane (1 mL) and an aliquot of each sample (2 μL) was injected into a GC-MS system.

Analysis of phthalates in air was carried out according to the method reported by the Ministry of Health, Labour and Welfare of Japan (2000). Sampling was done using an SP208-10L (GL Science, Tokyo, Japan) pump attached to an AERO cartridge SDB 400 (GL Science) with a sampling rate of 5 L/min for 24 h. After the addition of isotopically labeled internal standards (4 μg/mL, 25 μL), the collected phthalates were extracted with acetone (2 mL) by ultrasonication for 10 min. After centrifugation at 3,000 rpm for 5 min, the supernatant was collected. An aliquot of each sample (2 μL) was injected into a GC-MS system.

GC-MS analysis was performed on an Agilent 6890 N GC/5973 N MSD instrument (Agilent Technologies, CA, USA). A 30 m HP-5MS SV column (J & W Scientific, CA, USA) with 0.25 mm i.d. and 0.5 μm film thickness was used. The initial oven temperature was 80°C. After holding at the initial temperature for 2 min, the temperature was increased to 240°C at a rate of 40°C/min, and then to 300°C at a rate of 10°C/min, where it remained constant for 5 min. Helium was used as carrier gas at a flow-rate of 1.2 mL/min). The ion source temperature was 230°C and electron ionization was used as the ionization mode. The injection port was kept at 250°C. The ions used for selected ion monitoring are summarized in Table 1. DIOP was determined as the two highest peaks, and DINP as the five main peaks in the chromatogram as described by Tsumura et al. (2001).

Table 1 Retention times, quantification and confirmation ions for the measured phthalates: dibutyl phthalate, DBP; butyl benzyl phthalate, BBzP; di-2-ethylhexyl phthalate, DEHP; diisooctyl phthalate, DIOP; diisononyl

Analyte	Retention time (min)	Quantification ion	Confirmation ion
DBP	8.0	149	205, 223
DBP-d_4	8.0	153	209, 227
BBzP	10.2	149	91, 206
BBzP-d_4	10.2	153	91, 210
DEHP	11.3	149	167, 279
DEHP-d_4	11.3	153	171, 283
DIOP	11.5–12.1	149	279
DOP-d_4	12.5	153	283
DINP	12.8–13.9	149	293
DNP-d_4	14.2	153	297

Results and Discussion

The recoveries from diets and beddings spiked with 100 ng/g of DBP, BBzP and DEHP and 500 ng/g of DIOP and DINP were examined. Overall recoveries of the three repeated measurements are summarized in Table 2; these values were 98.8%–148% with coefficients of variation (CV) of 0.4%–7.8% for diets and 94.7%–146% with CV of 1.0%–5.0% for beddings. Recoveries of BBzP, DIOP and DINP were satisfactory (98.8%–113% for diets; 94.7%–119% for beddings); however, those of DBP and DEHP were relatively high (123%–148%).

The elimination of phthalate contamination is key for precise measurement. Blanks originating from sample analysis were therefore examined using phthalates-free water instead of diet and bedding. The blanks from diet sample analysis were 5.0 (±1.9) ng/g for DEHP, <3.0 ng/g for DBP and BBzP, and <20 ng/g for DIOP and DINP ($n = 5$), and those from bedding sample analysis were 6.6 (±2.5) ng/g for DEHP, 3.1 (±0.3) ng/g for DBP, <3.0 ng/g for BBzP, and <20 ng/g for DIOP and DINP ($n = 5$). The limit of quantification (LOQ) for each of five phthalates was calculated as $10S_0$, where S_0 is the value of the standard deviation obtained by analyzing quintuplicate sets of the blank analysis, or as $10S_1$, where S_1 is the value of the standard deviation obtained by analyzing quintuplicate sets of the lowest level of standard sample. The LOQ for each of five phthalates is summarized in Table 2. With our careful control of contamination, sample analysis was achieved with a low-level background, which allowed us to evaluate the amount of phthalates precisely. Typical chromatograms of a standard mixture and of diet and bedding samples are shown in Fig. 1.

Table 2 Recoveries and LOQ of phthalates

Analyte	Diet			Bedding		
	Recovery (%)	CV[a] (%)	LOQ[b] (ng/g)	Recovery (%)	CV (%)	LOQ (ng/g)
DBP	123	7.8	10	132	5.0	5
BBzP	98.8	0.4	10	102	1.0	10
DEHP	148	1.8	20	146	4.2	25
DIOP	109	0.5	50	119	4.3	50
DINP	113	1.3	50	94.7	4.3	50

Results are means of three replicate determinations

[a] *CV* coefficients of variation

[b] *LOQ* limit of quantification

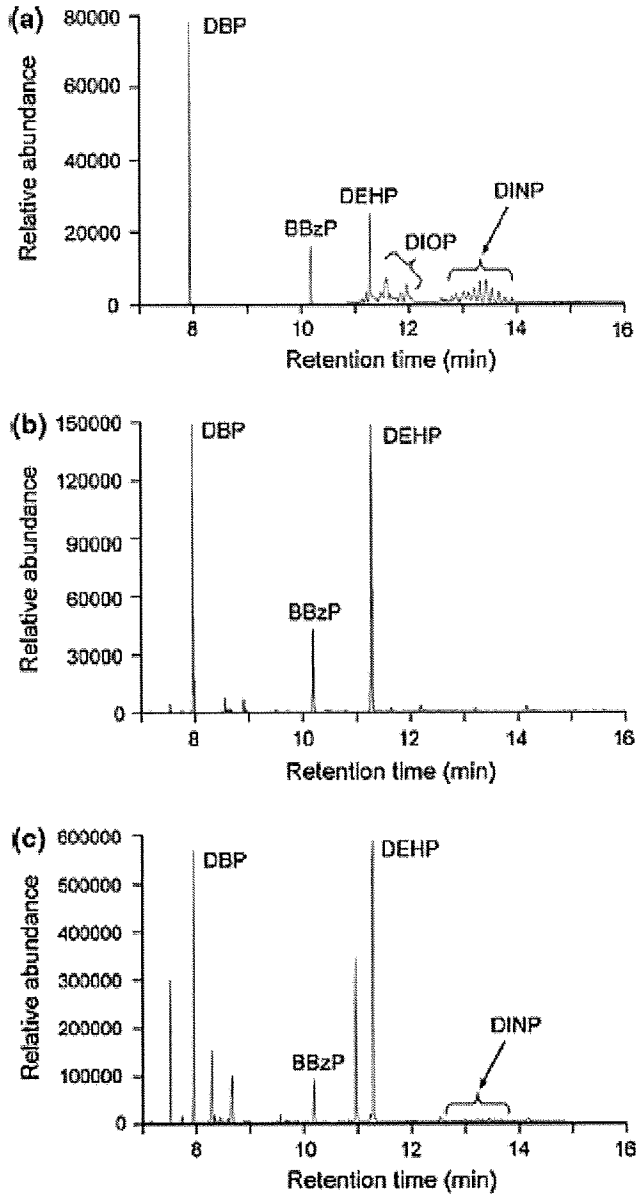

Fig. 1 Typical selected ion monitoring chromatograms of a a standard mixture of five phthalates, b diet and c bedding

We evaluated the suitability of the method for detecting the levels of phthalate in 12 commercial animal diets and 13 bedding materials (Table 3). All samples were analyzed just after opening the package. Two of the most frequently detected phthalates were DBP, which was found in all diets and beddings, and DEHP, which was found in all diets and in 77% of the beddings. BBzP was not detected in most samples (15%–33% detectable), and DINP was detected in only one sample of bedding. DIOP was not detected in any diet or bedding. The levels of phthalates varied from sample to sample; the concentrations of five phthalates were 141–1,410 ng/g for diets and 20.5–7,560 ng/g for beddings.

Table 3 Concentrations of phthalates in commercial animal diets and beddings (ng/g)

Sample no.	DEHP	DBP	BBzP	DIOP	DINP	Sum
Diet						
D1	143	179	<LOQ	<LOQ	<LOQ	322
D2	160	46.3	<LOQ	<LOQ	<LOQ	206
D3	116	25.1	<LOQ	<LOQ	<LOQ	141
D4	511	146	157	<LOQ	<LOQ	814
D5	156	41.4	<LOQ	<LOQ	<LOQ	197
D6	146	134	<LOQ	<LOQ	<LOQ	280
D7	118	36.1	<LOQ	<LOQ	<LOQ	154
D8	205	80.4	<LOQ	<LOQ	<LOQ	285
D9	281	205	22.2	<LOQ	<LOQ	508
D10	422	403	18.4	<LOQ	<LOQ	843
D11	257	344	<LOQ	<LOQ	<LOQ	601
D12	431	944	33.4	<LOQ	<LOQ	1,410
Bedding						
B1	449	1,380	<LOQ	<LOQ	<LOQ	1,830
B2	<LOQ	757	<LOQ	<LOQ	<LOQ	781
B3	280	19.6	<LOQ	<LOQ	<LOQ	300
B4	498	765	<LOQ	<LOQ	<LOQ	1,260
B5	<LOQ	6.0	<LOQ	<LOQ	<LOQ	20.5
B6	187	128	<LOQ	<LOQ	<LOQ	315
B7	262	130	440	<LOQ	<LOQ	832
B8	420	66.4	<LOQ	<LOQ	<LOQ	486
B9	132	538	<LOQ	<LOQ	<LOQ	670
B10	5,070	1,390	900	<LOQ	198	7,560
B11	547	381	<LOQ	<LOQ	<LOQ	928
B12	443	55.5	<LOQ	<LOQ	<LOQ	499
B13	<LOQ	30.5	<LOQ	<LOQ	<LOQ	46.5

Results are means of duplicate determinations

The results of our study demonstrated that the levels of phthalates varied from sample to sample. The highest value for the concentration of five phthalates in diets (1,410 ng/g) was 10 times higher than the lowest value. If a rat weighing 150 g eats 12 g of this diet daily (Poon et al. 1997), 16,920 ng of phthalates would be ingested, which corresponds to an oral administration of 0.113 mg/kg per day. The levels of phthalates in the diets analyzed in this study are about 20–2,000 times lower than those fed in reported developmental and reproductive toxicity experiments (Poon et al. 1997; Tyl et al. 1988; Arcadi et al. 1998). However, it is necessary to take into account the progress of the contamination during storage after opening the packaging of diets.

In terms of the contamination level in beddings, one sample (no. B10), made of recycled paper, showed a remarkable level of contamination at a concentration of

Table 4 Concentrations of five phthalates in water supplied to the animals, and samples of air taken from the animal room

Sample	DEHP	DBP	BBzP	DIOP	DINP	Sum
Water (ng/mL)						
Water1	<LOQ	<LOQ	<LOQ	<LOQ	<LOQ	<LOQ
Water2	<LOQ	<LOQ	<LOQ	<LOQ	<LOQ	<LOQ
Water3	<LOQ	<LOQ	<LOQ	<LOQ	<LOQ	<LOQ
Air (ng/m^3)						
Air1	31.4	357	<LOQ	<LOQ	<LOQ	388
Air2	27.6	320	<LOQ	<LOQ	<LOQ	348
Air3	31.9	261	<LOQ	<LOQ	<LOQ	293

Results are means of duplicate determinations

five phthalates of 7,560 ng/g. Although we cannot estimate the exposure to phthalates from beddings through oral intake by licking and dermal absorption, it would be better not to use heavily contaminated bedding to avoid the potential exposure to high levels of phthalates.

In order to investigate the other causes of rodent exposure to phthalates under various feeding conditions, we analyzed water supplied to the animals, and samples of air taken from the animal room (Table 4). None of the five phthalates was detected in the water (lower limits of quantification: DBP, BBzP and DEHP, 0.5 ng/mL; DIOP and DINP, 2 ng/mL). DBP and DEHP were detected in all samples of air with concentration ranges of 261–357 ng/m^3 and 27.6–31.9 ng/m^3, respectively. Other three phthalates were not detected (lower limits of quantification: BBzP, 5 ng/m^3; DIOP and DINP, 20 ng/m^3). The contamination level in air taken from the animal room was 293–388 ng/m^3 for five phthalates. The average exposure from air amounts to 101 ng/day when we assume an average daily inhalation of 0.29 m^3 air per rat (The ICH Steering Committee 1997). This level of exposure by inhalation would be about 125 times lower than the intake from diets. These results indicate that the major source of exposure to phthalates may be the diet, although the possibility cannot be denied completely that direct incorporation of these phthalates from the lung without hydrolysis occurs.

In summary, we have developed a GC-MS method to determine five phthalates in diets and beddings used for experimental animals. We analyzed commercial animal diets and beddings, and found that both of them were polluted by phthalates, especially DBP and DEHP, suggesting that dietary exposure to phthalates routinely occurs. The total exclusion of phthalates from the experimental environment is probably impossible. Therefore, the contamination levels in the diet and bedding should be measured. Additionally, it would be wise to monitor the contamination levels of water and the air in the animal room, although the exposure from water and air was low.

Acknowledgments This study was supported by a grant from the Ministry of Health, Labor, and Welfare, Japan.

References

Arcadi FA, Costa C, Imperatore C, Marchese A, Rapisarda A, Salemi M, Trimarchi GR, Costa G (1998) Oral toxicity of bis(2-ethylhexyl) phthalate during pregnancy and suckling in the Long-Evans rat. Food Chem Toxicol 36:963–970

Blount BC, Silva MJ, Caudill SP, Needham LL, Pirkle JL, Sampson EJ (2000) Levels of seven urinary phthalate metabolites in a human reference population. Environ Health Perspect 108:979–982

Duty SM, Silva MJ, Barr DB, Brock JW, Ryan L, Chen Z, Herrick RF, Christiani DC, Hauser R (2003) Phthalate exposure and human semen parameters. Epidemiology 14:269–277

Glick EM (1998) Liquid-liquid extraction gas chromatographic/mass spectrometric method. In: Clesceri LS, Greenberg AE, Eaton AD (eds) Standard methods for the examination of water and wastewater, 20th edn. APHA Press, North Wales, pp 6–59

Kato K, Silva MJ, Needham LL, Calafat AM (2005) Determination of total phthalates in urine by isotope-dilution liquid chromatography-tandem mass spectrometry. J Chromatogr. B 814:355–360

Ministry of Health, Labour and Welfare of Japan (2000) Committee on sick house syndrome: indoor air pollution progress report No. 1

Parks LG, Ostby JS, Lambright CR, Abbott BD, Klinefelter GR, Barlow NJ, Gray LE Jr (2000) The plasticizer diethylhexyl phthalate induces malformations by decreasing fetal testosterone synthesis during sexual differentiation in the male rat. Toxicol Sci 58:339–349

Poon R, Lecavalier P, Mueller R, Valli VE, Procter BG, Chu I (1997) Subchronic oral toxicity of di-n-octyl phthalate and di(2-ethylhexyl)phthalate in the rat. Food Chem Toxicol 35:225–239

Silva MJ, Barr DB, Reidy JA, Malek NA, Hodge CC, Caudill SP, Brock JW, Needham LL, Calafat AM (2004) Urinary levels of seven phthalate metabolites in the U.S. population from the National Health, Nutrition Examination Survey (NHANES) 1999–2000. Environ Health Perspect 112:331–338

Swan SH, Main KM, Liu F, Stewart SL, Kruse RL, Calafat AM, Mao CS, Redmon JB, Ternand CL, Sullivan S, Teague JL, the Study for Future Families Research Team (2005) Decrease in anogenital distance among male infants with prenatal phthalate exposure. Environ Health Perspect 113:1056–1061

Takatori S, Kitagawa Y, Kitagawa M, Nakazawa H, Hori S (2004) Determination of di(2-ethylhexyl)phthalate and mono(2-ethylhexyl)phthalate in human serum using liquid chromatography-tandem mass spectrometry. J Chromatogr B 804:397–401

The ICH Steering Committee. Impurities: guideline for residual solvents. International conference on harmonisation of technical requirements for registration of pharmaceuticals for human use. 17 July 1997

Tsumura Y, Ishimitsu S, Saito I, Sakai H, Kobayashi Y, Tonogai Y (2001) Eleven phthalate esters and di(2-ethylhexyl) adipate in one week duplicate diet samples obtained from hospitals and their estimated daily intake. Food Addit Contam 18:449–460

Tyl RW, Price CJ, Marr MC, Kimmel CA (1988) Developmental toxicity evaluation of dietary di(2-ethylhexyl)phthalate in Fischer 344 rats and CD-1 mice. Fundam Appl Toxicol 10:395–412

Journal of Reproduction and Development, Vol. 56, No. 1, 2010

—Full Paper—

Resistance to 5-aza-2′-deoxycytidine in Genic Regions Compared to Non-genic Repetitive Sequences

Hui Wen LIM[1)], Misa IWATANI[1)], Naoko HATTORI[1)], Satoshi TANAKA[1)], Shintaro YAGI[1)] and Kunio SHIOTA[1)]

[1)]*Laboratory of Cellular Biochemistry, Animal Resource Sciences/Veterinary Medical Sciences, The University of Tokyo, Tokyo 113-8657, Japan*

Abstract. The DNA methyltransferase (Dnmt) inhibitor and demethylating agent 5-aza-2′-deoxycytidine (5azadC) has been used to induce cellular differentiation and gene activation. It has been approved for treating several kinds of malignancies due to its ability to reactivate silenced tumor suppressor genes. Considering the potential effect of 5azadC on non-targeted genomic regions in normal cells, we investigated its effect on repetitive sequences and selected gene loci, *Oct-4*, *Sall3*, *Per1*, *Clu*, *Dpep1* and *Igf2r*, including tissue-dependent and differentially methylated regions, by treating mouse NIH/3T3 fibroblast cells with concentrations of 5azadC ranging from 0.001 to 5 μM. Demethylation of minor satellite repeats and endogenous viruses was concentration dependent, and the demethylation was strong at 1 and 5 μM. In genic regions, the methylation level decreased only at 0.1 μM, but was minimally altered at concentrations lower or higher, regardless of the abundance of CpG sites. Thus, repeats are strongly demethylated, but genic regions are only demethylated at effective doses. Genes were activated by 5azadC treatment and were accompanied by a unique combination of histone modifications in genic regions, including an increased level of H3K9me3 and a decreased level of AcH3. Increase of H3K9me3 in genic regions was not observed in Dnmt knock out cells. We identified differential effects of 5azadC on repetitive sequences and genic regions and revealed the importance of choosing appropriate 5azadC doses to achieve targeted gene recovery.

Key words: 5-aza-2′-deoxycytidine, Decitabine, DNA methylation, Epigenetics, Histone modification

(**J. Reprod. Dev.** 56: 86–93, 2010)

DNA methylation is one of the epigenetic events associated with gene regulation and function. Hypermethylation of promoter regions of tumor suppressor genes causes silencing of the genes that lead to cancer [1–3]. Thus, reversing the methylation status of gene promoters to their prevalent methylation states has become a treatment option for certain cancer types. To date, there are many types of demethylating agents that have been shown to inhibit promoter methylation and reactivate silenced genes [4–6]. Some of these have been approved or are in clinical studies to be developed as cancer drugs [7].

The cytosine analog 5-aza-2′-deoxycytidine (5azadC), also known as decitabine, has been widely used as a DNA methyltransferase (Dnmt) inhibitor to reverse aberrant hypermethylation [8, 9]. It has been approved for hematological malignancies, showing favorable results with low dose treatment [10, 11]. Known to have dual modes of action, 5azadC at low doses induces gene hypomethylation, whereas high doses of 5azadC induce cytotoxicity and cause severe side effects in patients [12, 13].

Nearly 40% of the mouse genome is composed of repetitive sequences including different classes of interspersed repeats, such as LINEs, SINEs, LTR elements and satellites, that are mainly found in heterochromatin regions [14]. Most repeats are densely methylated, and methylation in repeats reflects the global methylation level [15, 16]. Loss of methylation in repeats causes genomic instability [17, 18]. Conversely, genes comprise only a small portion of the genome. Tissue-dependent and differentially methylated regions (T-DMRs) are unique sequences in genic regions that are methylated depending on tissue or cell types. T-DMRs have been widely observed, including in undifferentiated embryonic stem cells, normal tissues and even in cloned mice [19–21]. Both repetitive regions and T-DMRs serve as important markers for methylation analysis, as repeats could be used to estimate global methylation, whereas T-DMRs could serve as references for cell- or tissue-specific methylation.

Previous reports show that Dnmts exhibit functional cooperation on genomic regions [22, 23]. We reported previously that Dnmt1, Dnmt3a and Dnmt3b share targets in the same CpG islands with T-DMRs, and each Dnmt has target preferences depending on the genomic regions [24]. Dnmt3a and Dnmt3b prefer T-DMRs of genic regions, whereas Dnmt1 prefers repetitive sequences.

The demethylating effect of 5azadC is exerted by binding to Dnmts [4]. Since Dnmts have multiple targets, there is the potential of having a genome-wide demethylating effect when using 5azadC. Demethylation of non-targeted genomic regions might occur, not only in cancer cells but also in normal cells. In addition, there are diverse interactions between DNA methylation and histone modifications in euchromatic and heterochromatic regions [25, 26]. The epigenetic status of T-DMRs is regulated by the interplay between DNA methyltransferases, histone modification enzymes, nuclear proteins and other epigenetic factors that cooperate to form cell- and tissue-specific DNA methylation profiles [27,

Received: March 17, 2009
Accepted: October 3, 2009
Published online in J-STAGE: December 9, 2009

Correspondence: K Shiota (e-mail: ashiota@mail.ecc.u-tokyo.ac.jp)

28]. It may be possible to induce hypomethylation-independent activation of gene expression and downstream responses. To know whether 5azadC induces an invariable effect on different genomic regions, we investigated the effect of 5azadC on non-genic repetitive sequences and some genic regions including T-DMRs in fibroblast cells.

Materials and Methods

Reagents, cell culture and genome extraction

All reagents were purchased from Wako Pure Chemicals (Osaka, Japan) unless stated otherwise.

NIH/3T3 cells were cultured in Dulbecco's modified Eagle's medium (DMEM; Invitrogen, Carlsbad, CA, USA) supplemented with 10% fetal bovine serum (JRH, Lenexa, KS, USA) and 50 unit/ml penicillin / 50 μg/ml streptomycin (Invitrogen) at 37 C in 5% CO_2 in air. Prior to treatment with 5-aza-2'-deoxycytidine (5azadC; Sigma-Aldrich, St. Louis, MO, USA; diluted with sterile water to the concentrations required), cells were plated at 1×10^5 cells/150 mm dish and cultured for 24 h. Cells were treated with 5azadC to final concentrations ranging from 0.001 to 5μM. Sterile water was substituted for 5azadC in the untreated control. The medium was changed every 24 h, and cells were collected after 3 days for DNA extraction.

Wild type ES cells (J1) and mutant ES cells deficient in *Dnmt*1 (*Dnmt*1$^{-/-}$; c/c), *Dnmt*3a and *Dnmt*3b (*Dnmt*3a$^{-/-}$3b$^{-/-}$; 7aabb) were cultured on gelatin coated dishes with ES medium containing 1000 U/ml leukemia inhibitory factor (Chemicon, Temecula, CA, USA) as previously described [24]. J1, c/c and 7aabb cells were harvested at passage numbers 32, 17 and 17, respectively.

Cells were incubated in lysis buffer (150 mM EDTA, 10 mM Tris-HCl, pH 8.0, and 1% SDS) containing 10 mg/ml proteinase K (Merck, Darmstadt, Germany) at 55 C for 20 min. Following phenol/chloroform/isoamyl alcohol extraction twice, genomic DNA was precipitated with ethanol and dissolved in TE buffer (10 mM Tris-HCl, 1 mM EDTA, pH 8.0).

Cell proliferation assay

NIH/3T3 cells were seeded into 96-well plates at 1×10^3 cells per well, 24 h before 5azadC was added. Cells were treated with 5azadC at final concentrations of 0 (as the control), 0.001, 0.005, 0.01, 0.05, 0.1, 0.5, 1.0, 5.0 and 10.0 μM for 3 or 4 days at 37 C in 0.5% CO_2 in air with medium changes every 24 h. Four hours before plate reading, 10 μl of Cell Proliferation Reagent WST-1 (Roche, Penzberg, Germany) was added. The absorbance of each sample was measured against a background control using an ELISA reader at an absorption wavelength of 450 nm.

Analysis of the methylation status of repetitive sequences by Southern blotting

Genomic DNA (5 μg) was digested with the restriction enzyme *Msp*I (Takara, Kyoto, Japan) or *Hap*II (Takara) and electrophoresed on a 0.8% agarose gel. Following hydrolyzation with 0.25 N HCl and denaturation with 1.5 M NaCl/0.5 N NaOH, the DNA was transferred onto a nylon membrane. The membrane was probed with pMO for endogenous C-type retrovirus (MoMuLV; Genbank accession NC_001501) and pMR150 for minor satellite repeats (X14469 and X07949). Probes were labeled with the Gene Images random prime labeling module (Amersham Pharmacia, Little Chalfont, Buckinghamshire, UK). Hybridization and detection were performed using the Gene Images CDP-star detection module (Amersham Pharmacia) according to the manufacturer's instructions.

Bisulfite restriction mapping and sequencing

Genomic DNA, digested with *Eco*RI, was denatured by incubating with 0.3 M NaOH at 37 C for 15 min. Sodium metabisulfite (pH 5.0) and hydroquinone were added to a final concentration of 2 M and 0.5 mM, respectively, and the mixture was incubated at 55 C for 18 h in the dark. Bisulfite modified DNA was purified with the Wizard DNA Clean-Up System (Promega, Madison, WI, US), and the bisulfite reaction was terminated with NaOH at a final concentration of 0.3 M at 37 C for 15 min. The sample was neutralized by adding NH_4OAc, pH 7.0 (3 M, final concentration), and was precipitated with ethanol. Purified DNA was dissolved in sterile water and amplified using Immolase (Bioline, Tokyo, Japan) with the primer sets as follows: 5'-TAAGGGTAGGTATATAGGTGTGGT-3', F, and 5'-TCTACCCCCTTTAAAAATCACTTTAA-3', R, for ODE; 5'-TGGGTTGAAATATTGGGTTTATTT-3', F, and 5'-CTAAAACCAAATATCCAACCATA-3', R, for OPR; 5'-GGGAAGGGGATTTTGTTATTGTAGT-3', F, and 5'-CATAAACCCAACAACAAACCCATCT-3', R, for *Per1*; 5'-GTTAGGGTTTTTTTAG-GGTATTAGT-3', F, and 5'-CCCTAATCTACCCAACATATACAAA-3', R, for *Sall3*. The PCR conditions were as follows: 95 C for 10 min, followed by 40 cycles of denaturation at 94 C for 30 sec, annealing at 55 C for 30 sec and extension at 72 C for 1 min, with a final extension at 72 C for 10 min.

Oct-4 distal enhancer, *Oct-4* proximal enhancer and promoter PCR products were digested with *Taq*I (Takara) at 65 C, and *Per*1 and *Sall*3 PCR products were digested with *Hpy*CH4IV (NEB, Ipswich, MA, USA) at 37 C for 3 h. Restricted fragments were assessed by agarose gel electrophoresis. Images were recorded and semi-quantified using the ImageJ software provided by the National Institutes of Health (http://rsbweb.nih.gov/ij/). The relative DNA methylation level of each genic region was calculated by the formula: DNA methylation status (%)=$100 \times I^C / (I^{UC} + I^C)$, where I^C and I^{UC} represent the intensities of the digested and undigested bands, respectively.

For bisulfite sequencing, PCR products were cloned into pGEM T-Easy vector (Promega, Madison, WI, USA), and 10 clones were sequenced for each sample. The primer sets used were 5'-TGGGCTGAAATACTGGGTTCACCC-3', F, and 5'-CTGAAGCCAGGTGTCCAGCCATG-3', R, for *Oct-4*; 5'- GGTTGGGGAATTGGTTGTT-3', F, and 5'-CAACCTACTCCTAAATCCTCCA-3', R, for *Dpep1*; 5'- TAGTGAGTGGGGATGTAGTATTATGG-3', F, and 5'-AACCCCTAAACAACTTCAAAATTTT-3', R, for *Clu*; and 5'-GTTTAGAATATTGGTGAGTAGTGGG-3', F, and 5'-CCTTAAAATAAAAATAAACATCTTAAA-3', R, for *Igf2r*, with the following PCR conditions: 95 C for 10 min, followed by 40 cycles of denaturation at 94 C for 30 sec, annealing at 55 C for 30 sec and extension at 72 C for 1 min, with a final extension at 72 C for 10 min.

RNA extraction and RT-PCR

Total RNA was extracted with TRIzol reagent (Invitrogen) according to the manufacturer's instructions. First strand cDNA was synthesized with SuperScript™ III First-Strand Synthesis System for RT-PCR (Invitrogen), and RT-PCR was performed using Taq DNA Polymerase (Promega) with primers as follows: 5'-CAGGAGTGTGTGAGGGAG-3', F, and 5'-GGTGTCACTGTCCGACTTGC-3', R, for *Dnmt1*; 5'-ACCCATGCCAAGACTCACCTTC-3', F, and 5'-TCCACCTTCTGAGACTCTCCAG-3', R, for *Dnmt3a*; 5'-TCAGACACGAAGGATGCTCC-3', F, and 5'-ACAGGGTACTCCTGCACATG-3', R, for *Dnmt3b*; 5'-TTCTACAATGAGCTGCGTGTGG-3', F, and 5'-ATGGCTGGGGTGTTGAAGGT-3', R, for *β-actin*; 5'-GGCGTTCGCTTTGGAAAGGTGTTC-3', F, and 5'-CTCGAACCACATCCTTCTCT-3', R, for *Oct-4*; 5'- CCAGTCGAAGATGCTCAACA-3', F, and 5'- TGTGATGGGGTCAGAGTCAA-3', R, for *Clu*; 5'- ATGCGGTATCTGACCCTCAC-3', F, and 5'-ATCTGCAAAGCGTCCTTCAT-3', R, for *Dpep1* and 5'-CAACGTCTGTGGAAATGTGG-3', F, and 5'- CAGCCCATAGTGGTGTTGAA-3', R, for *Igf2r*. The PCR conditions were as follows: 95 C for 1 min, followed by 30 cycles of denaturation at 94 C for 30 sec, annealing at 60 C for 30 sec and extension at 72 C for 1 min, with a final extension at 72 C for 5 min.

Chromatin immunoprecipitation (ChIP) assay

ChIP assays were performed as described previously [20] using a Chromatin Immunoprecipitation (ChIP) Assay Kit (Cat. No. 17-295; Upstate Biotechnology, Lake Placid, NY, USA) with anti-acetylated histone H3 and H4 antibodies (Cat. No. 06-599 and 06-598; Upstate Biotechnology), anti-trimethylated H3K4 and H3K9 (Cat. No. ab8580 and ab8898; Abcam, Cambridge, UK) and anti-dimethylated H3K4, H3K9 and H3K27 (Cat. No. 07-030, 07-212 and 07-452; Upstate Biotechnology). Normal rabbit IgG (Cat. No. 12-370; Upstate Biotechnology) was used as a negative control to verify immunoprecipitation specificity. PCR was performed using primers as follows: 5'- GTGAGGTGTCCGGTGACCCAAGGCAG-3', F, and 5'- CGGCTCACCTAGGGACGGTTTCACC-3', R, for *Oct-4*; 5'- TGCTCTGGAGACACAGGAAA-3', F, and 5'-CTGGGGAAGAAAGCCAAGAT-3', R, for *Clu* ChIP 1; 5'-ATTGCAGTGATGCCAGATGA-3', F, and 5'- ACGCACAGCAGGAGAATCTT-3', R, for *Clu* ChIP 2; 5'-CTCCTCTTGTGGCTCCCTAA-3', F, and 5'-GGCTCCACAGAGTGCCAAG-3', R, for *Dpep1*. PCR was performed under the following conditions: 95 C for 10 min, followed by 30 cycles of denaturation at 94 C for 30 sec, annealing at 55 C for 30 sec and extension at 72 C for 1 min, with a final extension at 72 C for 10 min. The amount of each PCR product on an ethidium bromide-stained gel image was evaluated using the ImageJ software.

Results

Demethylating effect of 5azadC on repetitive sequences

We examined cell survival under different concentrations of 5azadC by WST-1 assay. After 72 h, the viable cell number was largely reduced at concentrations higher than 0.5 μM and was severely affected at higher concentrations (Fig. 1A). A similar effect was observed in the 96-h culture. Only minimal effects on viability were observed in cells treated with less than 0.1 μM 5azadC.

To determine the effect of 5azadC on the methylation of repetitive sequences, cells were treated with 0.001 μM to 5 μM 5azadC, and the methylation status of repetitive sequences was analyzed using methylation-sensitive restriction enzymes. Southern hybridization was performed using two probes of differentially localized repetitive sequences, minor satellite repeats located in the centromeric regions and endogenous C-type viruses interspersed across the mouse genome [14, 24, 29]. Minor satellite repeats were demethylated extensively starting at the 0.1 μM concentration (Fig. 1B), and 1 μM was sufficient to induce the maximum demethylating effect. Similarly, endogenous viruses showed aggressive loss of methylation at the 0.1 μM to 5 μM treatment levels, but slight demethylation could be observed at a concentration as low as 0.001 μM. Thus, the repetitive sequences were strongly demethylated by 5azadC. The results confirmed a previous report that 5azadC is effective in inducing demethylation dose-dependently from 0.1 μM to 5 μM [30].

Effect of 5azadC on genic regions

We next examined the effect of 5azadC on T-DMRs of genic regions. *Oct-4* (*Pou5f1*) has T-DMRs in the CpG-rich promoter/proximal enhancer region and distal enhancer region (Fig. 1C; 20). The DNA methylation status of the T-DMRs was analyzed using bisulfite restriction mapping focusing on *Taq*I restriction sites. At 0.001 and 0.01 μM 5azadC, the methylation levels of the investigated regions changed little compared to the untreated ones. A significant loss of methylation in both regions was observed at 0.1 μM, indicating that this concentration was able to induce demethylation in both genic regions and the repetitive sequences. In the 1 and 5 μM treated samples, however, both T-DMRs had nearly the same methylation levels as in the untreated control, in contrast to the extensive demethylation observed in the repetitive sequences at these concentrations.

Sall3 has a T-DMR located at an edge of a CpG island, which is methylated only in the trophoblast cell lineage [19, 21]. The T-DMR is aberrantly methylated in the placental genome of cloned mice [21]. *Per1*, which is involved in generating circadian rhythm, has a few CpGs in the upstream promoter region. Similar to *Oct-4*, 0.001 and 0.01 μM 5azadC had minimal effects on these loci. The methylation levels decreased significantly following 0.1 μM 5azadC treatment, but were only slightly decreased at 1 μM, and remained unchanged at 5 μM.

Bisulfite sequencing was performed on several gene loci containing CpG-rich promoters, including *Oct-4*. Hypomethylation of the *Clusterin (Clu)* promoter is associated with high gene expression in the rat testis and epididymis [31]. *Dpep1*, a renal *Dipeptidase* gene, has been reported to be a tumor marker candidate in malignancies [32]. All investigated loci had hypermethylated promoter regions in NIH/3T3 cells (Fig. 2A). Bisulfite sequencing results for the *Oct-4* promoter region validated the restriction mapping results showing that 0.1 μM was more effective in inducing demethylation in genic regions compared with 1 μM. Similar dose-dependent demethylation patterns were also

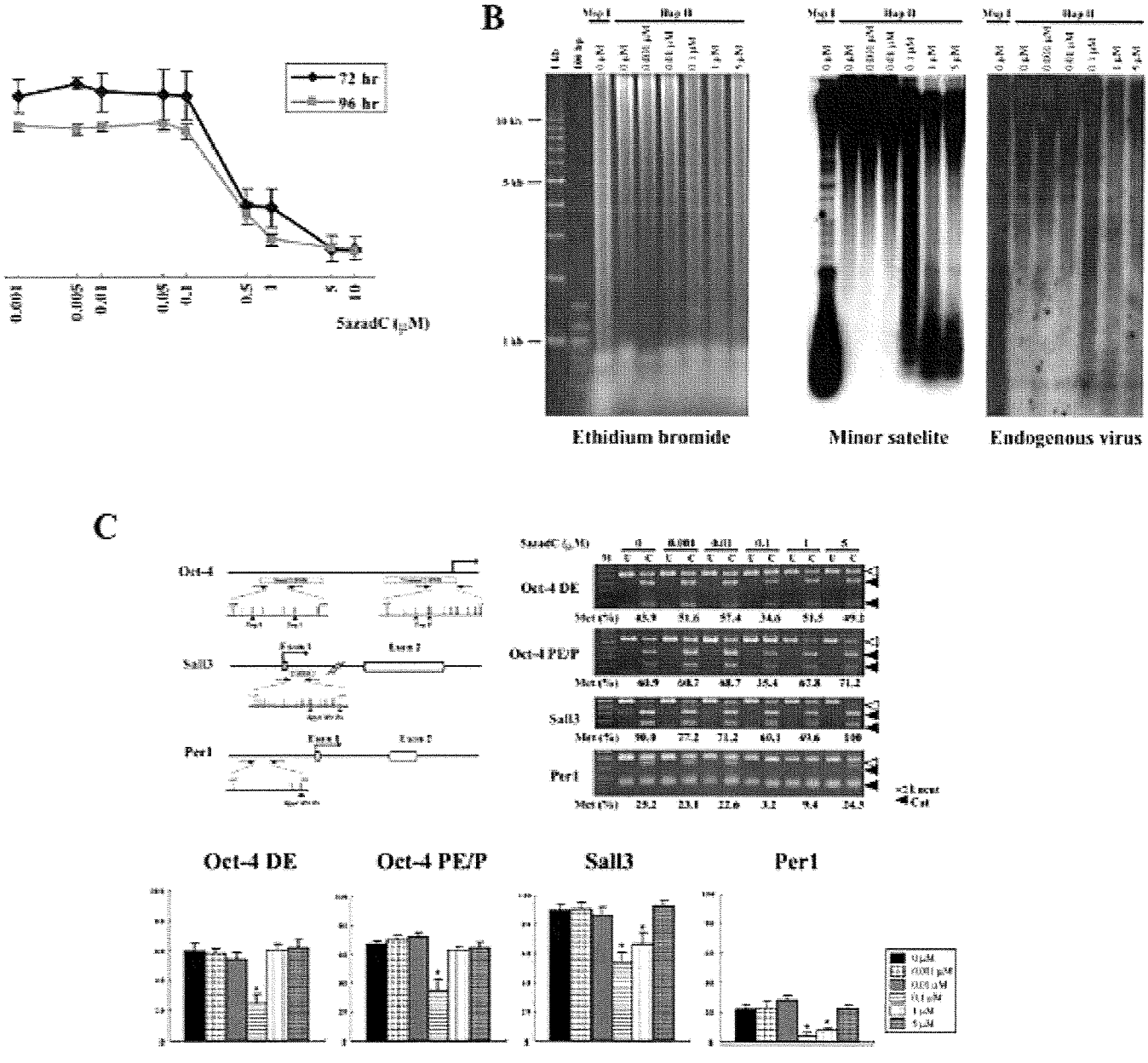

Fig. 1. Different demethylating effects of 5azadC on repetitive sequences and genic regions. A: A WST-1 cell proliferation assay was performed on cells treated with 5azadC at the indicated concentrations for 72 and 96 h. Cell number was estimated by the absorbance, and then represented as the ratio relative to the untreated control, the absorbance of which was arbitrarily set to 100. The values represent means ± S.E. of 3 independent cultures. B: Analysis of the methylation status of repetitive sequences by Southern hybridization. Genomic DNA (5 μg), digested with *HapII*, was hybridized to probes for minor satellite repeats and endogenous viruses. As a control for complete digestion, DNA from the untreated control was digested with *MspI*. C: Methylation analysis of T-DMRs by bisulfite restriction mapping. A schematic diagram of each investigated locus is shown in the top left panel. T-DMRs are represented by bars, and CG sites are represented by vertical lines. The locations of the amplified regions relative to each respective transcription start site are as follow: *Oct-4* distal enhancer (DE), -3086 to -2646; *Oct-4* proximal enhancer/promoter (PE/P), -420 to +31; *Sall3*, +1253 to +1665; and *Per1*, -1087 to -929. Each locus contains 2 *TaqI* or *Hpy*CH4IV restriction sites, respectively (triangles). PCR products were digested with restriction enzymes and electrophoresed on agarose gel (top right panel). The relative DNA methylation level was calculated based on the relative intensities of cut to uncut bands, indicated below each cut lane. M, marker; U, uncut; C, cut with restriction enzyme. The bottom panel indicates the methylation level of each gene locus at each concentration; the values are presented as means ± S.E. of 3 independent PCRs of 2 cultures. * P<0.05 (Student's *t*-test).

observed in the promoter regions of *Clu* and *Dpep1*.

We also analyzed the DMR2 region of the *Igf2r* imprinted gene, which is differentially methylated depending on its parental origin [33]. Due to allele-specific methylation, half of the clones were methylated in the untreated control. As observed in other genes, the DMR2 region appeared demethylated at 0.1 μM, but was not affected by 1 μM 5azadC.

These results provide evidence that 5azadC has a strong demethylating effect on repetitive sequences, but its effect on genic regions is limited to a certain effective dose. The expression levels